



**HAL**  
open science

# Advances in Surface Passivation of Nanoscale Zerovalent Iron A Critical Review

S. Bae, R.N. Collins, T.D. Waite, K. Hanna

► **To cite this version:**

S. Bae, R.N. Collins, T.D. Waite, K. Hanna. Advances in Surface Passivation of Nanoscale Zerovalent Iron A Critical Review. Environmental Science and Technology, American Chemical Society, 2018, 52 (21), pp.12010-12025. 10.1021/acs.est.8b01734 . hal-01939031

**HAL Id: hal-01939031**

**<https://hal-univ-rennes1.archives-ouvertes.fr/hal-01939031>**

Submitted on 14 Dec 2018

**HAL** is a multi-disciplinary open access archive for the deposit and dissemination of scientific research documents, whether they are published or not. The documents may come from teaching and research institutions in France or abroad, or from public or private research centers.

L'archive ouverte pluridisciplinaire **HAL**, est destinée au dépôt et à la diffusion de documents scientifiques de niveau recherche, publiés ou non, émanant des établissements d'enseignement et de recherche français ou étrangers, des laboratoires publics ou privés.

# Advances in surface passivation of nanoscale zerovalent iron (NZVI): A critical review

Sungjun Bae,<sup>†</sup> Richard N. Collins,<sup>‡</sup> T. David Waite<sup>‡</sup> and Khalil Hanna<sup>\*,§</sup>

<sup>†</sup>Department of Civil and Environmental Engineering, Konkuk University, 120 Neungdong-ro,  
Gwangjin-gu, Seoul 05029, Republic of Korea

<sup>‡</sup>School of Civil and Environmental Engineering, University of New South Wales, Sydney,  
New South Wales 2052, Australia

<sup>§</sup>Univ Rennes, Ecole Nationale Supérieure de Chimie de Rennes, CNRS, ISCR –  
UMR6226, F-35000 Rennes, France

\*Corresponding author: Tel.: +33 2 23 23 80 27; fax: +33 2 23 23 81 20.

E-mail address: khalil.hanna@ensc-rennes.fr (K. Hanna)

A revised review submitted to *Environmental Science and Technology*

September, 2018

**24 ABSTRACT**

25       Nanoscale zerovalent iron (NZVI) is one of the most extensively studied nanomaterials in  
26 the fields of wastewater treatment and remediation of soil and groundwater. However, rapid  
27 oxidative transformations of NZVI can result in reduced NZVI reactivity. Indeed, the surface  
28 passivation of NZVI is considered one of the most challenging aspects in successfully  
29 applying NZVI to contaminant degradation. The oxidation of NZVI can lead to the formation  
30 of Fe<sup>II</sup>-bearing phases (e.g., Fe<sup>II</sup>O, Fe<sup>II</sup>(OH)<sub>2</sub>, Fe<sup>II</sup>Fe<sup>III</sup><sub>2</sub>O<sub>4</sub>) on the NZVI surface or complete  
31 oxidation to ferric (oxyhydr)oxides (e.g., Fe<sup>III</sup>OOH). This corrosion phenomenon is dependent  
32 upon various factors including the composition of NZVI itself, the type and concentration of  
33 aqueous species, reaction time and oxic/anoxic environments. As such, the co-existence of  
34 different Fe oxidation states on NZVI surfaces may also, in some instances, provide a unique  
35 reactive microenvironment to promote the adsorption of contaminants and their subsequent  
36 transformation via redox reactions. Thus, an understanding of passivation chemistry, and its  
37 related mechanisms, is essential not only for effective NZVI application but also for  
38 accurately assessing the positive and negative effects of NZVI surface passivation. The aim of  
39 this review is to discuss the nature of the passivation processes that occur and the passivation  
40 byproducts that form in various environments. In particular, the review presents: i) the  
41 strengths and limitations of state-of-the-art techniques (e.g., electron microscopies and X-ray  
42 based spectroscopies) to identify passivation byproducts; ii) the passivation mechanisms  
43 proposed to occur in anoxic and oxic environments; and iii) the effects arising from synthesis  
44 procedures and the presence of inorganics/organics on the nature of the passivation  
45 byproducts that form. In addition, several depassivation strategies that may assist in  
46 increasing and/or maintaining the reactivity of NZVI are considered, thereby enhancing the  
47 effectiveness of NZVI in contaminant degradation.

48

## 49 1. INTRODUCTION

50 In recent decades, zerovalent iron (ZVI, Fe(0)) has been extensively studied for its  
51 capacity to transform contaminants in soils, groundwater and industrial wastewaters because  
52 of: (i) its ability to reductively transform a wide variety of compounds, such as halogenated  
53 organics, into less toxic and/or more biodegradable forms; (ii) the abundance of iron (the  
54 fourth most abundant element in the earth's crust); (iii) the relative environmental friendliness  
55 of an iron-based technology compared to other zerovalent metals (such as Mn(0) and Cu(0))  
56 and (iv) the low cost of Fe<sup>0</sup> mass production.<sup>1-7</sup> In particular, nanoscale zerovalent iron (NZVI)  
57 has attracted attention due to the potential advantages arising from high particle reactivity  
58 (resulting from the small size and high surface area of NZVI) when compared to ZVI.<sup>3-6,8-21</sup>  
59 Moreover, NZVI has been confirmed to reductively remove various organic (e.g., chlorinated  
60 aliphatic<sup>3,6,8-10</sup> and aromatic compounds<sup>10,11,13,14</sup>), inorganic (e.g., nitrate,<sup>12</sup> Cr(VI),<sup>17</sup> As(III)<sup>18-</sup>  
61 <sup>22</sup> and Cd(II)<sup>23</sup>) and radioactive (e.g., U(VI)<sup>24-26</sup> and Tc(VII)<sup>27</sup>) contaminants under anoxic  
62 conditions. It has also been demonstrated that NZVI can induce the oxidative degradation of  
63 organic contaminants (e.g., pharmaceuticals<sup>28,29</sup> and herbicides<sup>30,31</sup>). This may occur as a  
64 result of the reduction of dissolved oxygen (O<sub>2</sub>) and the associated production of hydrogen  
65 peroxide (H<sub>2</sub>O<sub>2</sub>) that subsequently reacts with Fe(II) (that is also produced during oxidation)  
66 leading to initiation of the Fenton reaction (Fe(II) + H<sub>2</sub>O<sub>2</sub> → Fe(III) + HO\* + OH<sup>-</sup>) and the  
67 generation of strongly oxidizing hydroxyl radicals (HO\*, 2.80 V).

68 Typical NZVI particles have a core-shell (Fe(0)-Fe (oxyhydr)oxide) structure with the  
69 spherical nanosized primary particles forming chain-like aggregates with sizes ranging up to a  
70 few micrometers.<sup>3</sup> Moreover, the aggregates exhibit the magnetic properties of the primary  
71 particles with the magnetism of the primary particles influencing the size and structure of  
72 these assemblages.<sup>32</sup> The co-existence of the Fe(0) core and oxidized Fe surface layer  
73 provides a unique reactive surface for the initial adsorption of contaminants and their

74 subsequent transformation on the particle surface via reductive or oxidative  
75 pathways.<sup>3,5,14,16,29,30</sup> In accordance with contaminant adsorption, oxidation or reduction, Fe  
76 may undergo oxidation (from Fe(0) to Fe(II) and Fe(II) to Fe(III)), precipitation (as Fe(II)  
77 and/or Fe(III) solids) and, possibly, co-precipitation with ionic species.<sup>8,33–35</sup> Concomitantly,  
78 it may also be necessary to consider reactions with other solution phase entities such as O<sub>2</sub>,  
79 (which, as noted above, may be reduced to H<sub>2</sub>O<sub>2</sub>, possibly due to adsorption to NZVI or its  
80 (oxyhydr)oxide-coated surface),<sup>28,29</sup> sulfate (which may possibly be reduced to sulfide,  
81 resulting in the formation of FeS solid phases on the NZVI surface)<sup>35</sup> and carbonate (which  
82 may also promote the precipitation of ferrous carbonate minerals).<sup>36</sup>

83 Many researchers have demonstrated that NZVI undergoes surface oxidation (or surface  
84 passivation) when used for the removal of contaminants in variably oxic environments.<sup>3,6,8,29</sup>  
85 In addition, a field study has shown that 78–97% of Fe(0) injected was oxidized in a sediment  
86 sample after 165 d at a remedial site contaminated with a dense non-aqueous phase liquid  
87 (DNAPL).<sup>37</sup> Investigations have revealed that, depending on the environmental conditions  
88 and types of contaminants present, NZVI surface layers (and eventually, the bulk of the solid)  
89 transform to different Fe mineral phases, such as vivianite (Fe<sup>II</sup><sub>3</sub>(PO<sub>4</sub>)<sub>2</sub>·8H<sub>2</sub>O), Fe(OH)<sub>2</sub>,  
90 green rust (Fe(II)-Fe(III) layered double hydroxides with various interlayer anions (e.g. Cl<sup>-</sup>,  
91 SO<sub>4</sub><sup>2-</sup> and CO<sub>3</sub><sup>2-</sup>)), ferrihydrite, magnetite (Fe<sup>II,III</sup><sub>2</sub>O<sub>4</sub>), lepidocrocite (γ-Fe<sup>III</sup>OOH), goethite (α-  
92 Fe<sup>III</sup>OOH), mackinawite (Fe<sup>II</sup>S), and siderite (Fe<sup>II</sup>CO<sub>3</sub>), as presented in Table 1. Moreover,  
93 NZVI can be completely transformed to lepidocrocite in oxygenated water<sup>38</sup> and partially  
94 transformed to Fe(OH)<sub>2</sub> in O<sub>2</sub>-free water in the absence of contaminants.<sup>39</sup> The passivation  
95 kinetics and the nature of the products generated have a significant influence on the long-term  
96 viability of the technology given that Fe(II)-containing minerals such as magnetite,<sup>40–43</sup>  
97 vivianite,<sup>44–47</sup> and green rust<sup>48–50</sup> and surface-bound Fe(II)<sup>51,52</sup> can further remove organic and  
98 inorganic contaminants. In addition, Fe(III)-containing minerals (e.g., maghemite (γ-Fe<sub>2</sub>O<sub>3</sub>),<sup>53</sup>

99 goethite<sup>54</sup> and hematite<sup>55</sup>) can effectively remove contaminants via sorptive effects. For  
100 example, it has been reported that, in anoxic conditions, passivated NZVI demonstrated  
101 similar or slightly higher sorptive ability for perfluoroalkyl acids<sup>56</sup> and As(V)<sup>57</sup> when  
102 compared to fresh NZVI. These results are most likely due to the presence of a greater  
103 number of adsorption sites on the Fe (oxyhydr)oxides passivating the NZVI surface compared  
104 to the number of sites on pristine NZVI. These findings imply that passivation byproducts of  
105 NZVI can potentially act as reactants for the further removal of contaminants, even after the  
106 depletion of the initial NZVI.

107 Although the positive effects of passivation are evident, there are several adverse effects  
108 to the formation of passivation byproducts on NZVI that should be considered (in addition to  
109 reduced activity). The production of reactive oxygen species (ROS) in NZVI suspensions, as  
110 previously mentioned, was considered to account for the high toxicity of fresh NZVI to rodent  
111 neuron and microglia cells when compared to the limited effect of aged NZVI and magnetite  
112 nanoparticles<sup>58</sup> with the severity of toxicity related to the iron oxidation state with Fe(0) >  
113 Fe(II) > Fe(III).<sup>59</sup> The toxicity of passivation byproducts from NZVI may be lower than that  
114 of NZVI however the results of the above studies suggest that the passivation byproducts (i.e.,  
115 Fe(II) and Fe(III) species) can also induce secondary toxic effects. In addition, it has been  
116 suggested that the presence of nanoparticles may enhance the transport of contaminants  
117 associated with these nanoparticles,<sup>60</sup> though certain reports suggest that the mobility of NZVI  
118 particles is likely to be retarded as a result of the association of these particles with subsurface  
119 sediments.<sup>61,62</sup> Therefore, an understanding of passivation kinetics, transformation byproducts  
120 and related mechanisms is required when considering the reactivity, longevity and stability of  
121 NZVI.

122 Although a number of reviews regarding NZVI have been published, most reviews have  
123 focused on NZVI synthesis and characterization, application to the removal of contaminants

124 or implementation and results of field studies.<sup>15,63-74</sup> In comparison, in this review, we  
125 introduce: (i) common characterization techniques for determining the nature of passivation  
126 byproducts; (ii) insights into the passivation mechanism(s) underlying observed structural  
127 transformations of NZVI in oxic and anoxic environments and (iii) the effect of synthesis  
128 methods and solution conditions such as the presence of various organic and inorganic species  
129 on the passivation process. In addition, we describe various depassivation strategies that could  
130 potentially be used to either prevent or retard passivation processes and thereby extend the  
131 lifetime over which NZVI is an effective agent for the degradation of contaminants.

132

## 133 **2. CHARACTERIZATION OF NZVI PASSIVATION BYPRODUCTS**

134 To identify the NZVI passivation mechanism operating under specific conditions, the  
135 investigation and monitoring of the formation of passivation byproducts throughout and after  
136 the passivation process are required. In this section, common techniques used for identifying  
137 passivation byproducts are reviewed and the benefits and limitations of each technique are  
138 discussed. The primary methods of interest include electron microscopy, X-ray diffraction  
139 (XRD), X-ray photoelectron spectroscopy (XPS), Raman and Mössbauer spectroscopies and  
140 X-ray absorption spectroscopy (XAS).

141

### 142 **2.1. Electron Microscopy**

143 Transmission and scanning electron microscopy (TEM and SEM) have been the most  
144 widely used techniques to determine the morphological characteristics of NZVI passivation  
145 byproducts. TEM can provide visual information at the nanoscale level of properties such as  
146 the core size of fresh NZVI, the thickness of the passivating layer after partial passivation, and  
147 morphological changes after complete structural transformation. Additionally,  
148 crystallographic information including crystallinity and lattice spacing can be obtained using

149 selected area electron diffraction.<sup>36,39</sup> For fresh NZVI, a spherically-shaped core-shell  
150 structure is commonly observed using TEM. The size of the core is typically within a range of  
151 tens of nanometers with the core covered by a thin Fe (oxyhydr)oxide layer of several  
152 nanometers thickness as shown in Figure S1.<sup>3,8,19,38,75</sup> After surface passivation,  
153 morphological changes in the NZVI structure can be detected using TEM. Typical changes  
154 include loss of the Fe(0) core and the appearance of hollow (oxyhydr)oxide shells with this  
155 transformation reported to occur within 24 h under oxic conditions.<sup>38</sup> Further aging to 72 h  
156 can result in the formation of flake- or acicular-shaped minerals (such as lepidocrocite).<sup>38</sup>

157 Another effective analytical technique typically associated with TEM is X-ray energy  
158 dispersive spectroscopy (XEDS). The results of XEDS can provide the elemental composition  
159 of passivation byproducts and can support identification of the Fe mineral phases present,  
160 especially when certain elements such as P and S are co-localised in minerals such as  
161 (respectively) vivianite ( $\text{Fe}_3(\text{PO}_4)_2$ ) and mackinawite ( $\text{FeS}$ ).<sup>33,34,35</sup> In recent times, scanning  
162 TEM (STEM)-XEDS has been used to identify the passivation mechanism that occurs in  
163 single nanoparticles by the acquisition of nanoscale images and elemental maps.<sup>36,38,76</sup> For  
164 instance, the growth of amorphous assemblages within the NZVI core with subsequent  
165 transformation to plate-like crystalline forms has been observed using STEM (Figures 1(a-c)).  
166 These results can then be matched to XEDS maps to reveal a decrease and increase,  
167 respectively, in the Fe and O contents within the NZVI core.<sup>36</sup>

168

## 169 **2.2. X-ray Diffraction (XRD)**

170 X-ray diffraction is one of the most popular analytical techniques for characterizing the  
171 particular minerals that form upon NZVI passivation.<sup>15</sup> It is particularly useful for identifying  
172 crystalline phases that give sharp and characteristic diffraction peak patterns. Most studies in  
173 which the mineralogy of passivated NZVI has been examined by XRD have typically been



174 limited to analyses ‘before’ and ‘after’ reaction of the sample with very limited insight gained  
175 into the kinetics of mineral transformations.<sup>22,77–79</sup> A large number of iron crystalline phases  
176 have been identified by XRD in passivation byproduct studies however lepidocrocite and  
177 magnetite/maghemite are overwhelmingly the dominant phases detected.<sup>15</sup> The latter two  
178 minerals cannot be identified separately by XRD as both have indistinguishable diffraction  
179 patterns despite their different oxidation states. Other less common NZVI passivation  
180 byproducts detected by XRD include ferrihydrite,<sup>77</sup> goethite,<sup>80</sup> vivianite,<sup>33,34</sup> amakinite  
181 ( $\text{Fe}^{\text{II}}(\text{OH})_2$ ),<sup>81</sup> hematite,<sup>18</sup> chukanovite ( $\text{Fe}^{\text{II}}_2(\text{OH})_2\text{CO}_3$ )<sup>82</sup> and carbonate green rust.<sup>83</sup>

182 Perhaps the most significant limitation of using XRD to identify passivation byproducts  
183 is that some minerals, including NZVI itself, quite often present as X-ray amorphous and/or  
184 only display broad diffraction peaks.<sup>15</sup> In addition, the mineral detection limits for XRD are in  
185 the order of 2 to 3 wt. %.<sup>15</sup> Thus, quantitative analysis of the relative proportions of minerals  
186 present could be difficult or impossible with this analytical approach. This could possibly  
187 explain why the very common nanocrystalline, X-ray amorphous mineral ferrihydrite has  
188 rarely been identified as a major passivation byproduct in NZVI studies in which XRD was  
189 used as the primary characterization technique.

190

### 191 **2.3. X-ray Photoelectron Spectroscopy (XPS)**

192 X-ray photoelectron spectroscopy is a surface sensitive technique that can be used to  
193 characterize several nanometers of the NZVI outer layer. Although it is difficult to  
194 conclusively determine the nature of the NZVI passivation byproducts using XPS due to the  
195 limited information that can be obtained on the mineral phases, this technique can provide  
196 important information on the nature of the elements present at the NZVI surface including  
197 their oxidation states. The kinetic energy and number of electrons emitted from irradiation of  
198 the surface by X-rays of known energy are measured during XPS analysis. For the

199 determination of the oxidation state of elements present within the surface layer, the narrow  
200 peaks for the Fe(2p<sub>3/2</sub>) and O(1s) binding energies are particularly useful.<sup>8,40,84</sup> A  
201 comprehensive understanding of the oxidation states of the Fe and O species on the NZVI  
202 surface can provide critical information on passivation byproducts.<sup>38,84–86</sup> For example, the  
203 presence of an Fe(0) peak at ~706 eV indicates that the core Fe(0) is preserved because XPS  
204 is sensitive to the outermost layer of the particles.<sup>6</sup> In addition, it has been reported that after  
205 72 h reaction with oxygenated water, NZVI passivation byproducts displayed peaks of Fe at  
206 ~711 eV and O at ~530 eV and 531 eV, indicating the presence of Fe<sub>2</sub>O<sub>3</sub>, Fe<sub>3</sub>O<sub>4</sub> and/or  
207 FeOOH.<sup>38</sup>

208

#### 209 **2.4. Raman and Mössbauer Spectroscopies**

210 Raman spectroscopy can be carried out *in situ* to monitor the formation of NZVI  
211 passivation byproducts, particularly when the minerals to be identified are poorly crystalline.  
212 However, the transformation of Fe (oxyhydr)oxides as a result of laser-induced thermal  
213 heating may complicate interpretation of results.<sup>77</sup> For example, hematite is often detected by  
214 Raman spectroscopy but absent in corresponding XRD data.<sup>77,78</sup> In the early stages of NZVI  
215 aqueous oxic corrosion, wustite (Fe<sup>II</sup>O) can be detected by Raman spectroscopy (~595 cm<sup>-1</sup>)<sup>78</sup>.  
216 It is an unstable intermediate phase generally formed in small amounts below the  
217 detection limit of XRD. At longer aging times (e.g. 30 d in static deionized water or 24 h in  
218 deionized water mixed at 300 rpm), Raman analyses have revealed the simultaneous co-  
219 existence of maghemite (665 and 730 cm<sup>-1</sup>), magnetite (670 cm<sup>-1</sup>) and lepidocrocite (650 cm<sup>-1</sup>).<sup>77,78</sup>  
220 On prolongation of NZVI aging time to 60–90 d in static water or 48–72 h in stirred  
221 water, only lepidocrocite (250, 380, 526 and 650 cm<sup>-1</sup>) was identified (in close agreement  
222 with XRD results).<sup>38</sup> Raman analysis has been used to show that aging under anoxic  
223 conditions favors the formation of wustite, goethite and akaganeite (β-Fe<sup>III</sup>OOH).<sup>78</sup>

224 <sup>57</sup>Fe Mössbauer spectroscopy can be used for detecting Fe atoms in different oxidation  
225 states and is a useful technique to identify the nature of any amorphous mineral phases present.  
226 Mössbauer spectroscopy can provide relevant information on the valency and spin states of Fe  
227 species as well as their magnetic properties via analysis of the hyperfine parameters. As such,  
228 magnetite and maghemite can be distinguished using this technique. Moreover, it can be used  
229 to determine the percentages of elemental Fe(0) and other secondary minerals that are  
230 present.<sup>63</sup> The typical <sup>57</sup>Fe Mössbauer spectrum of ZVI exhibits a single magnetic component  
231 corresponding to Fe(0) with hyperfine parameters corresponding to a cubic phase of metallic  
232 Fe. However a simple spectrum of this nature has rarely been observed for NZVI, even when  
233 the NZVI was pristine and freshly- prepared.<sup>19,63,87</sup> Typically, a complex hyperfine structure is  
234 observed with at least five components: a magnetic sextet with narrow lines corresponding to  
235 that of Fe(0), two quadruple components corresponding to Fe(III) and Fe(II) species, and two  
236 magnetic components. Mössbauer specialists suggest that these results are indicative of the  
237 presence of disordered ferric (oxyhydr)oxides (e.g., Fe(OH)<sub>3</sub>) and/or superparamagnetic ferric  
238 oxides (e.g., Fe<sub>3</sub>O<sub>4</sub>) on the passivated surface of Fe(0). When NZVI reacts with contaminants  
239 in water, a quadruple doublet and a magnetic sextet with broadened lines are commonly  
240 observed and have generally been attributed to the formation of lepidocrocite and a mixture of  
241 magnetite and maghemite, respectively.<sup>19,87</sup>

242

## 243 **2.5. X-ray Absorption Spectroscopy (XAS)**

244 Despite the widespread use in the fields of geochemistry and material science, XAS has  
245 had a limited application in NZVI studies with only a handful of studies describing the use of  
246 this technique to characterization of NZVI<sup>15,33,88,89</sup> or NZVI passivation byproducts.<sup>36,79,86,90–92</sup>  
247 One of the great strengths of Fe K-edge XAS is that it can provide quantitative insight into all  
248 the iron minerals present. This is because the high energy of the Fe K-edge (7112 eV for

249 Fe(0)), allows for the entirety of the particles to be sampled by the beam. As an XAS  
250 spectrum is a linear combination of its components, it can then be fitted with reference  
251 material spectra in a linear least-squares fitting manner using software such as ATHENA.<sup>93</sup>  
252 As recommended elsewhere,<sup>67</sup> the choice of reference material spectra and the number of  
253 components to fit sample spectra should be guided on evidence from complementary  
254 analytical techniques, knowledge of the NZVI system, or principle component analysis and  
255 target analysis.

256 In the NZVI studies mentioned above, either the X-ray absorption near-edge structure  
257 (XANES) or extended X-ray absorption fine structure (EXAFS) regions of the XAS spectrum  
258 have been modelled. Generally, the Fe K-edge XANES region can be used for fitting spectra  
259 when there are multiple Fe oxidation states present.<sup>86,89-91</sup> However, it is a less useful region  
260 to distinguish between Fe(III) oxyhydroxide passivation byproducts. For example, the  
261 XANES spectra of ferrihydrite, lepidocrocite and goethite can, for fitting purposes, be  
262 practically identical when using a Si(111) monochromator. If the identity of the exact Fe(III)  
263 oxyhydroxides is an important component of a NZVI study, then the EXAFS region is better  
264 suited for fitting of data.<sup>36,92</sup> Interestingly, all the XAS studies that have examined NZVI  
265 passivation byproducts have done so under oxidative conditions. Nevertheless, as noted in  
266 many other NZVI studies, lepidocrocite, magnetite and maghemite are the main secondary  
267 iron minerals that have been detected by XAS analysis<sup>36,79,90-92</sup> though ferrihydrite and  
268 goethite have also been reported.<sup>36,79,92</sup>

269

### 270 3. NZVI PASSIVATION PROCESSES UNDER ANOXIC AND OXIC CONDITIONS

271 In this section, we review the state of knowledge with regard to the mechanism of  
272 passivation of NZVI under both anoxic and oxic conditions. Under anoxic conditions, the  
273 reaction with water is expected to be of principal importance for the formation of passivating

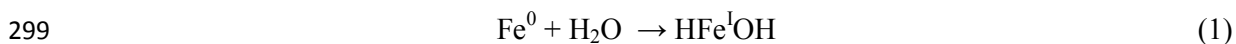
274 layers on the NZVI surface though attention is also given to the impact of other major  
275 solution constituents (such as carbonate, sulfate and nitrate) that may be present. Under oxic  
276 conditions, the presence of oxygen is obviously the major differentiator to anoxic systems  
277 with O<sub>2</sub> potentially influencing the reaction pathway of Fe(II) resulting from NZVI corrosion.  
278 Consideration is also given to the impact of the nature of the NZVI particle on the oxic  
279 passivation process with bimetallic particles of major interest.

280

### 281 **3.1. Anoxic Conditions**

282 With respect to the anoxic reaction of NZVI with water, the identification of the  
283 primary reductive products (particularly Fe(OH)<sub>2</sub> and magnetite) and the definition of the  
284 reaction mechanism have been well addressed by Filip et al.<sup>39</sup> These investigators<sup>39</sup>  
285 used “NANO FER 25P” NZVI particles of ~60 nm in diameter and a specific surface area of  
286 ~36 m<sup>2</sup>g<sup>-1</sup> that were thermally synthesized from iron oxide powder in H<sub>2</sub>. Aging studies were  
287 undertaken under strictly anoxic conditions at both 25 °C and 80 °C. <sup>57</sup>Fe Mossbauer  
288 spectroscopy indicated that approximately 70% of the Fe(0) was transformed to Fe(OH)<sub>2</sub> after  
289 ~3000 h of reaction at 25 °C with this mineral transforming relatively rapidly (after ~200 h) to  
290 magnetite (Fe<sub>3</sub>O<sub>4</sub>) at 80 °C (Figure 2). Interestingly, the results obtained by Filip et al.<sup>39</sup> were  
291 at odds with the results of earlier workers such as Reardon et al.<sup>94</sup> who concluded that  
292 magnetite was also formed at 25 °C. Filip et al.<sup>39</sup> investigated this discrepancy and showed  
293 that the nanosheets of Fe(OH)<sub>2</sub> formed in their study could be rapidly transformed to  
294 magnetite on exposure to air during analysis by XRD – the solid characterization method used  
295 by Reardon et al.<sup>94</sup>. Quantum chemical calculations indicated a two-step reaction mechanism  
296 involving two one electron transfer processes; the first, which involved the breakage of the H-  
297 O bond of water, can be described by the reaction (Eq.1):

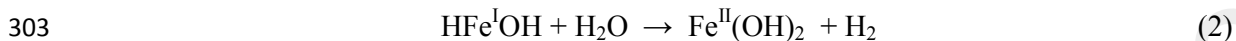
298



300

301 which represents the rate-limiting step, and the second by (Eq.2):

302



304

305 Filip et al.<sup>39</sup> note that the existence of the HFeOH molecule has previously been demonstrated  
306 (by Zhang et al.<sup>95</sup>) by argon matrix isolation FTIR spectroscopy.

307 The nature of the corrosion products formed on NZVI upon exposure to anoxic solutions  
308 has been investigated in a more recent study with Liu et al.<sup>78</sup> concluding that the major  
309 passivation byproducts formed after 72 h of reaction were wüstite ( $\text{Fe}^{\text{II}}\text{O}$ ), goethite and  
310 akageneite (Figure 3). These products differ markedly from those reported by Filip et al.<sup>39</sup> and  
311 beg the question of whether air exposure during TEM, XRD and Raman analyses resulted in  
312 transformation of the passivation products formed under anoxic conditions. Pullin et al.<sup>79</sup>  
313 investigated the nature of the passivation byproducts formed on exposure of NZVI to Milli-Q  
314 water for periods of more than four weeks with the nature of the passivation byproducts  
315 investigated by XAS. Amorphous passivation products (assigned as ferrihydrite) were formed  
316 within one day of exposure with the concurrent formation of magnetite. Over periods of up to  
317 four weeks, maghemite was observed to form with this oxide transforming slowly to “meta-  
318 stable” lepidocrocite. Over longer periods (greater than four weeks), all NZVI transformed to  
319 goethite with this iron oxide considered to be the likely “final state”

320 In summary, the anoxic corrosion of NZVI by water is dependent upon various factors,  
321 such as reaction time and temperature, with the major corrosion products observed being  
322 wüstite, goethite and magnetite. It should be recognized, however, that the intrusion of  
323 oxygen either through the aging process or during analysis may confound the results of

324 experiments undertaken under supposed anoxic conditions. As such, investigators should pay  
325 particular attention to the possibility of unintended NZVI passivation during studies under  
326 anoxic conditions.

327

### 328 **3.2. Oxic Conditions**

329 The nature of the oxidation products formed on exposure of nanometer-sized Fe(0)  
330 particles to oxygen has been of interest for many years in view of the widespread use of  
331 ultrafine magnetic particles in magnetic recording, ferrofluids and catalysis with the nature of  
332 the oxide phases formed on exposure of small iron particles to an oxygen-containing  
333 atmosphere investigated by a number of groups.<sup>96</sup> Linderoth et al.<sup>96</sup> found, using Mössbauer  
334 spectroscopy, that the oxide layer grows quickly initially then slows down with the oxide  
335 layer consisting of a mixture of Fe<sub>3</sub>O<sub>4</sub> and  $\gamma$ -Fe<sub>2</sub>O<sub>3</sub>. The kinetics of oxide layer formation  
336 followed a logarithmic rate law in accord with the Cabrera-Mott model of oxidation<sup>97</sup> with  
337 multistage steps including i) dissociative adsorption of O<sub>2</sub> at the metal surface, ii) oxidation of  
338 surface metal ions, iii) incorporation of metal ions into the oxide layer, iv) diffusion of metal  
339 ions in the oxide layer, and v) reaction of metal ions with oxygen ions with the diffusion of  
340 metal ions in the oxide layer considered to be rate limiting.<sup>98</sup>

341 In comparison with the logarithmic behavior of oxide layer growth revealed from  
342 studies of passivation of iron particles in air, investigations of the oxidation of Fe(0) surfaces  
343 in the presence of water vapour reveal that reactions at the iron surface/water interface are rate  
344 limiting with an initial lag in oxide layer formation followed by an exponential increase in  
345 growth of the oxide layer.<sup>99-101</sup> Investigation of the aging of iron nanoparticles in aqueous  
346 solution by Sarathy et al.<sup>102</sup> revealed similar behavior with Fe(0) nanoparticles from Toda  
347 (RNIP-10DS) becoming more reactive (as determined by the rate of carbon tetrachloride  
348 (CCl<sub>4</sub>) reduction) between 0 and ~2 days after exposure to water then gradually losing

349 reactivity over the ensuing 100 days. These changes in reactivity were correlated with  
350 evidence for destruction of an Fe(III) oxide film that initially covered the Fe(0) nanoparticles  
351 with subsequent formation of a new passivating mixed valence Fe(II)-Fe(III) oxide shell.<sup>102</sup>

352 Using quartz crystal microbalance measurements to quantify the rate of oxide layer  
353 formation, Greenlee et al.<sup>103</sup> showed similar behavior to that observed by Sarathy et al.<sup>102</sup> with  
354 an initial lag in oxide layer formation following by an exponential increase in mass of this  
355 layer (Region 1 in Figure S2). Decrease in water content of the solutions used (by replacing  
356 water with ethanol) resulted in an increase in the lag period before oxidation commenced and  
357 a decrease in the rate once oxidation had begun with these results confirming the critical role  
358 of H<sub>2</sub>O in destabilizing the passivating layer initially present. As shown in Figure S2, this  
359 exponential increase in oxide layer growth was followed by a logarithmic decline in rate of  
360 corrosion at later times (Region 2) with this behavior in accord with the Cabrera-Mott model  
361 described above. Greenlee et al.<sup>103</sup> showed that NZVI oxidized primarily to lepidocrocite with  
362 both carboxymethylcellulose (CMC) stabilizer and Ni slowing down the onset and extent of  
363 NZVI oxidation. Dong et al.<sup>104-106</sup> also showed that CMC and Ni slowed the aging of NZVI  
364 with the major products of oxidation found to be magnetite and maghemite.

365 Recent studies of NZVI-mediated oxidation by He et al.<sup>36</sup> confirmed the results of  
366 earlier studies by Joo et al.<sup>30</sup> that both Fe(II) and H<sub>2</sub>O<sub>2</sub> are generated following 1 h exposure  
367 of NZVI to oxygenated water at circumneutral pH. The solid Fe species resulting from  
368 exposure of NZVI to oxygen were examined, as a function of exposure time, by EXAFS  
369 spectroscopy.<sup>36</sup> Linear combination fitting of the EXAFS results indicated that NZVI  
370 transformed to lepidocrocite via an intermediate ferrihydrite phase following exposure of  
371 NZVI to oxygenated water with essentially all NZVI transformed to ferric oxyhydroxides  
372 after two hours of exposure to the oxic aqueous environment (Figure 1d).<sup>36</sup>



373 In summary, crystalline iron (oxyhydr)oxides such as lepidocrocite, maghemite and  
374 magnetite appear to be the major products formed upon the oxic corrosion of NZVI.  
375 Ferrihydrite may form initially but Fe(II)-catalyzed transformation to more crystalline forms  
376 is likely to occur as a result of the high concentrations of surface-associated Fe(II) present.  
377 The particular iron (oxyhydr)oxide formed is likely to be a function of the molar ratio of Fe(II)  
378 to Fe(III) surface sites present with the relatively short lifetime of Fe(II) in these oxic systems  
379 also influencing the extent of crystallization.

380

#### 381 4. FACTORS INFLUENCING NZVI PASSIVATION

382 Most of the published literature to date has addressed the impact of synthesis  
383 methods<sup>107</sup> and both organic and inorganic compounds<sup>4,33,80,108–117</sup> on the reactivity of NZVI  
384 with respect to target contaminants in the context of groundwater or wastewater remediation.  
385 In these studies, variations in the kinetic rate constants or extents of degradation were used as  
386 a means of assessing reactivity changes upon exposure to different cations or anions.  
387 However, very few attempts have been made to determine the corrosion mechanism(s) and to  
388 relate reactivity changes to the nature of the passivation byproducts formed<sup>107</sup> and the surfaces  
389 exposed to co-occurring solutes.<sup>33,80</sup>

390

##### 391 4.1. Effect of Synthesis Methods

392 The elemental composition of NZVI can vary depending on the synthesis method  
393 used,<sup>117,118</sup> which may influence NZVI reactivity as well as the nature of the passivation  
394 byproducts. In most cases, Fe reduction is mediated by NaBH<sub>4</sub> (NZVI<sup>BH</sup>) or H<sub>2</sub> (NZVI<sup>H2</sup>)  
395 (Table 1). The XPS results revealed that the NZVI<sup>H2</sup> surfaces composed of Fe (37.9–50.9%),  
396 O (44.2–52.9%), B (0%), Na (0.7–8.1%) and S (0.9–1.9%, possibly from the FeSO<sub>4</sub>  
397 precursor).<sup>107</sup> The surface of the NZVI<sup>BH</sup> particles contained less Fe (20.0%–30.8%) and S

398 (0.0%–0.5%), but greater O (49.1–59.2%), B (12.0–16.0%) and Na (0.5–14.5%).<sup>107,118</sup>  
399 Moreover, it was found that the S on the NZVI<sup>BH</sup> surface was in an oxidized form, whereas  
400 the S present on the surface of the NZVI<sup>H2</sup> particles was in reduced form.<sup>107</sup> Interestingly,  
401 NZVI<sup>H2</sup> exhibited lower reactivity than NZVI<sup>BH</sup> for the transformation of CCl<sub>4</sub> to chloroform  
402 (CHCl<sub>3</sub>), presumably due to the high Fe/O ratio (possibly associated with the presence of a  
403 magnetite shell) on the NZVI<sup>H2</sup> surfaces.<sup>107</sup> This hypothesis was supported by the low ability  
404 of nanoscale magnetite to transform CCl<sub>4</sub>.<sup>119</sup> These results serve to demonstrate that synthesis  
405 methods could alter the surface reactivity of NZVI and potentially its passivation mechanism.

406 As noted above, the use of NaBH<sub>4</sub> during the synthesis of NZVI<sup>BH</sup> can result in the  
407 occurrence of B on the surface of NZVI<sup>BH</sup>.<sup>120</sup> Recently, it has been reported that NaBH<sub>4</sub> can  
408 induce the disintegration of NZVI<sup>BH</sup> particles, resulting in the formation of significantly  
409 smaller particles.<sup>121</sup> This phenomenon may be induced by chemical etching of the passivated  
410 NZVI surface (coated, for example, by iron oxides such as magnetite) with this result  
411 consistent with the ability of NaBH<sub>4</sub> to induce the disintegration of microscale magnetite into  
412 nanoscale magnetite.<sup>122</sup> Although these authors did not compare their results to NZVI<sup>H2</sup>, the  
413 disparity in elemental surface composition (e.g., more Fe and S with less Na on the NZVI<sup>H2</sup>  
414 surfaces) may possibly cause reactions to proceed differently.

415

#### 416 4.2. Effect of Inorganic Compounds

417 Although the corrosion rate of NZVI and the nature of the passivation byproducts can be  
418 significantly affected by the presence of anionic or cationic inorganic species, very few  
419 studies have focused on this topic.<sup>33,80</sup> The corrosion phenomenon is dependent on several  
420 factors including the type and concentration of aqueous species, reaction time and oxic/anoxic  
421 environments.<sup>33,80</sup> It has been reported that the presence of common groundwater anions may  
422 promote or inhibit the corrosion of NZVI, however limited insight into the mechanism(s) of

423 the effects of anions is available.<sup>33,80</sup> After six months of aging in pH unbuffered and anoxic  
424 solutions containing 10 mM of either  $\text{HCO}_3^-$ ,  $\text{SO}_4^{2-}$ ,  $\text{NO}_3^-$ ,  $\text{HPO}_4^{2-}$  or  $\text{Cl}^-$ , NZVI (commercial  
425 sample, RNIP 10-DP) was found to predominantly transform to vivianite in the phosphate-  
426 aged sample and schwertmannite in the sulfate-aged sample (Figure S3).<sup>33</sup> Both the fresh  
427 NZVI and the sample aged for six months in 10 mM nitrate predominantly contained Fe(0)  
428 and magnetite.<sup>33</sup> The pH of the suspensions containing the different anions ranged from 9.0–  
429 11.8, indicating that the observed transformations occurred under alkaline conditions.<sup>33</sup> Using  
430 the same concentrations of the anionic species, NZVI<sup>H2</sup> particles have also been found to  
431 undergo corrosion into different iron phases after 16 weeks.<sup>80</sup> For example,  $\text{HCO}_3^-$  produced  
432 goethite,  $\text{NO}_3^-$  resulted in the formation of magnetite/maghemite and  $\text{SO}_4^{2-}$  and  $\text{Cl}^-$  produced  
433 a mixture of magnetite/maghemite, lepidocrocite and goethite (Figure S4).<sup>80</sup> It was observed  
434 that the corrosion rate of NZVI increased in the order  $\text{HCO}_3^- > \text{Cl}^-/\text{SO}_4^{2-} > \text{NO}_3^-$ , however  
435 pH was only measured in experiments in which the uptake of Cu and Zn by the corroded  
436 NZVI was examined over a time period of 4 weeks.<sup>80</sup> As such, the influence of this critical  
437 parameter on the nature of the formed passivation byproducts is unknown. Elsewhere, Kim et  
438 al.<sup>117</sup> have reported that a commercial NZVI (NANO FER 25DS) coated by S-based inorganic  
439 compounds was oxidized to magnetite in a synthetic groundwater containing  $\text{Cl}^-$  (1.95 mN),  
440  $\text{HCO}_3^-$  (1.14 mN),  $\text{NO}_3^-$  (0.15 mN) and  $\text{SO}_4^{2-}$  (0.44 mM). In contrast, iron carbonate hydroxide  
441 hydrate was detected as a major passivation byproduct in the presence of humic acid (2.5 mg  
442  $\text{L}^{-1}$ ).

443 Xie and Cwiertny<sup>4</sup> have reported that the presence of  $\text{Cl}^-$ ,  $\text{SO}_4^{2-}$  and  $\text{ClO}_4^-$  almost  
444 completely inhibited the reduction of 1,1,1,2-tetrachloroethane by NZVI over a time period of  
445 one month, irrespective of the nature or concentration of the anion present or pH. In contrast,  
446 the longevity toward degrading this contaminant was dependent upon the concentrations of  
447  $\text{NO}_3^-$  and  $\text{HCO}_3^-$  with complete reactivity loss over 1 d and 14 d, respectively, in 25 mM

448 suspensions. In addition, XRD analyses suggested that the loss in reactivity in  $\text{NO}_3^-$   
449 suspensions resulted from  $\text{Fe}(0)$  conversion into magnetite, whereas the formation of iron  
450 carbonate hydroxide limited reactivity in the  $\text{HCO}_3^-$  suspensions (Figure 4). Furthermore, Liu  
451 et al.<sup>108</sup> reported that trichloroethylene (TCE) reduction rates by NZVI are highly dependent  
452 on anion concentrations. For example, concentrations below 1 mM  $\text{NO}_3^-$  slightly increased the  
453 reduction rate but the reaction was retarded at  $\text{NO}_3^-$  concentrations between 1 and 3 mM and  
454 ceased at 5 mM. It was speculated that high  $\text{NO}_3^-$  concentrations may shift the TCE reduction  
455 reaction from one of cathodic control (i.e., the reduction of TCE) to anodic control (i.e., the  
456 release of  $\text{Fe}^{2+}$  and electrons) resulting in significant surface passivation.

457 On the other hand, Su et al.<sup>109</sup> reported that the rate of degradation of hexachlorobenzene  
458 by NZVI was not influenced by the presence of  $\text{HCO}_3^-$ ,  $\text{Mg}^{2+}$  or  $\text{Na}^+$  (over the concentration  
459 range of 0.8–7.7 mM). However, the rate of degradation was enhanced in the presence of 7.7  
460 mM  $\text{Cl}^-$  or  $\text{SO}_4^{2-}$  due to the promotion of corrosion but inhibited in the presence of 7.7 mM of  
461  $\text{NO}_3^-$  due to the competition between the anions and contaminants for reactive surface sites.  
462 However, it has been observed that the addition of  $\text{Na}_2\text{SO}_4$  inhibited the degradation of  
463 pentachlorophenol (PCP) by Pd/Fe bimetallic nanoparticles in the range of 2.5–10 mM<sup>110</sup> and  
464 the decolorization of methyl orange by NZVI particles at 14 mM.<sup>111</sup> Researchers generally  
465 attribute the inhibitory effects of common groundwater anions to their affinity for surface sites  
466 on the iron (oxyhydr)oxides coating the NZVI with the resulting surface complexes limiting  
467 the ability of contaminants to associate with the surface. Consistently, the inhibition effect has  
468 been found to increase in the order of  $\text{Cl}^- < \text{SO}_4^{2-} < \text{HPO}_4^{2-}$  for nitrate reduction by Peerless  
469  $\text{Fe}(0)$ <sup>112</sup> and  $\text{Cl}^- < \text{SO}_4^{2-} < \text{HCO}_3^- < \text{HPO}_4^{2-}$  for TCE reduction by NZVI.<sup>108</sup>

470 Given that the standard reduction potential of  $\text{Na}^+$  ions (-2.71 V) is below that of  $\text{Fe}^{2+}$   
471 ions (-0.44 V),  $\text{Na}^+$  ions do not affect degradation reactions mediated by  $\text{Fe}(0)$ .<sup>109</sup> However,  
472  $\text{Cu}^{2+}$  (0.8–7.7 mM) has been shown to enhance the degradation kinetics of hexachlorobenzene

473 by NZVI whereas  $\text{Fe}^{2+}$  (0.8–7.7 mM) has been reported to inhibit the degradation reaction due  
474 to the formation of passivation layers on the particle surfaces.<sup>109</sup> Moreover,  $\text{Cu}^{2+}$  (5–10 mM),  
475  $\text{Ni}^{2+}$  (5–10 mM) and  $\text{Fe}^{3+}$  (1.67–5 mM) have been observed to enhance PCP degradation by  
476 Pd/Fe nanoparticles due to the deposition of reduced copper and nickel species on the Fe  
477 surfaces.<sup>110</sup> The standard reduction potentials of the  $\text{Cu}^{2+}$  (+0.34 V) and  $\text{Ni}^{2+}$  (–0.257 V)  
478 cations are significantly higher than that of  $\text{Fe}^{2+}$  (–0.44 V) and, as such, the reduction of  $\text{Cu}^{2+}$   
479 or  $\text{Ni}^{2+}$  ions to their elemental forms is thermodynamically favorable.<sup>113,114</sup> In the case of the  
480  $\text{Fe}^{3+}$  cation, the enhancement observed in the PCP degradation was attributed to a decrease of  
481 pH resulting from the addition of the iron salt.<sup>110</sup> Furthermore, spectroscopic investigations of  
482 the structural evolution of NZVI in anoxic  $\text{Co}^{2+}$  solutions revealed that  $\text{Co}^{2+}$  was  
483 heterogeneously reduced ( $E_0 = -0.28$  V) and migrated to the NZVI core leading to its  
484 continuous removal from the solution.<sup>115</sup> However, information on whether  $\text{Co}^{2+}$  affects the  
485 nature of passivation byproducts is lacking though dissolution of sheet or shell structures upon  
486 metal complexation on the Fe surface has been reported in depassivation studies of micro-  
487 scale ZVI (~70 mesh) by Liu et al. (Figure 5).<sup>85,116</sup>

488 In summary, anionic ligands such as phosphate, silicate and sulfate may be readily  
489 adsorbed onto iron corrosion products, affecting the reactivity of NZVI particles. Hard cations  
490 (such as  $\text{Ca}^{2+}$  and  $\text{Mg}^{2+}$ ) and transition cationic metals (such as  $\text{Ni}^{2+}$ ,  $\text{Cu}^{2+}$  and  $\text{Co}^{2+}$ ) may  
491 exhibit promotive or inhibitive effects depending on their properties. However, the main  
492 secondary iron minerals formed during the reduction reaction have rarely been identified.

493

### 494 **4.3. Effect of Organic Compounds**

495 The use of organic ligands in NZVI studies has been investigated in the context of  
496 colloidal stabilization to increase particle mobility and improve redox reactivity. For example,  
497 chemical stabilizers (such as humic acid, polyacrylic acid and anionic or nonionic surfactants)

498 have been used to increase electrostatic repulsion effects and the stability of NZVI  
499 particles.<sup>16,20,123,124</sup> However, minimal attention has been given to the impact of stabilizers on  
500 the passivation of NZVI.

501 In oxygenated solutions, NZVI can undergo four electron transfer steps leading to the  
502 formation of reactive species such as HO<sup>\*</sup> and Fe(IV), which can potentially be utilized in the  
503 oxidative degradation of certain organic contaminants. The addition of iron-chelating agents  
504 such as oxalate, nitrilotriacetic acid, ethylenediaminetetraacetic acid, tetrapolyphosphate and  
505 polyoxometalate may accelerate the formation of ROS by mediating electron transfer from  
506 NZVI to oxygen (e.g., changing the four-electron transfer process to a two-electron transfer  
507 process) and by forming soluble complexes with iron at neutral pH values.<sup>125–127</sup> Although  
508 these studies did not assess the NZVI passivation byproducts in the presence of iron  
509 complexing agents and O<sub>2</sub>, the acceleration of the NZVI corrosion rate is expected under such  
510 conditions.

511 The effects of short chain organic acids (e.g., formic, oxalic and citric acid) on nitrate  
512 reduction by Fe(0) has been observed to increase in accordance with the degree to which the  
513 ligands adsorb to the surface of iron (oxyhydr)oxides or the stability constants of the aqueous  
514 complexes between Fe(III) and the organic ligands.<sup>112</sup> The blockage of reactive sites on the  
515 surface of Fe(0) and its passivation byproducts by the adsorption of ligands through an inner-  
516 sphere complexation mechanism may be responsible for the observed decrease in reduction  
517 rate. Unfortunately, information on whether and/or how the specific adsorption of ligands to  
518 the outer layers of corrosion products may alter the ongoing passivation or structural  
519 evolution of NZVI is very scarce.

520

## 521 5. DEPASSIVATION STRATEGIES

522 As discussed in the previous sections, most NZVI studies have focused on the  
523 passivation of NZVI after its use in water decontamination reactions. A decrease in NZVI  
524 reactivity is considered one of the major issues and a solution is required if NZVI is to be  
525 used to effectively degrade contaminants. In this section, a variety of depassivation strategies  
526 (including physical, chemical and biological approaches) are introduced to enhance and/or  
527 prolong the reactivity of NZVI. Particular attention is given to the use of depassivation  
528 strategies before, during and after the decontamination process.

529

### 530 **5.1. Depassivation before decontamination**

531 A well-known limitation to the broad application of NZVI for contaminant degradation is  
532 rapid pyrophoric reaction in air and surface passivation in aqueous solutions. This has led to  
533 studies examining possible synthesis procedures that can be used to produce reactive NZVI,  
534 i.e., NZVI that is atmospherically stable<sup>86</sup> or stable in aqueous phase.<sup>128</sup> For example, the  
535 shell-modified NZVI particles produced by Kim et al.<sup>86</sup> after controlled air-oxidation at  
536 various flow rates for 1 d did not ignite upon later exposure to atmospheric conditions.  
537 Shorter and longer controlled oxidation times resulted in spontaneous combustion or  
538 significantly decreased TCE degradation rates, respectively.<sup>86</sup> The optimal shell-modified  
539 NZVI particles exhibited a TCE degradation rate that was 78% of that obtained for fresh  
540 NZVI (Figure S5). It was also revealed that after aging in water for 1 d, both the fresh and  
541 shell-modified NZVI exhibited similar TCE degradation rate constants. It was conjectured  
542 that surface depassivation of the shell-modified particles was the cause for this observation,  
543 however, no mechanisms were examined or postulated.

544 It has been reported that annealing can induce structural and chemical changes in NZVI,  
545 with re-ordering and recrystallization of the inner Fe core, so as to eliminate defects and  
546 impurities.<sup>129</sup> In this case, the thickness of the surface oxide layer decreased from 3–4 nm to 2

547 nm by vacuum annealing at 500 °C with an accompanying change of the surface oxide from  
548 magnetite to wüstite and the migration of boron and carbon to the particle surface.<sup>129</sup> This  
549 depassivation process was postulated to improve the corrosion resistance and reactive lifespan  
550 of NZVI for environmental applications. A subsequent study performed by this group  
551 revealed that NZVI reactivity was significantly enhanced (by a factor of 30), with respect to  
552 the degradation of TCE and cis-1,2-dichloroethene, when compared to that of fresh NZVI due  
553 to efficient electron transfer from Fe(0) to the contaminants.<sup>130</sup>

554 In recent years there has been an explosion of interest in the sulfidation of NZVI during  
555 its synthesis to prevent surface passivation reactions that result from the reduction of water.  
556 Using variations of the method first outlined by Kim et al.,<sup>128</sup> several studies have revealed  
557 that sulfidated NZVI is superior to NZVI in decontamination reactions.<sup>35,128,131</sup> Enhanced  
558 decontamination by sulfidated NZVI has been hypothesized to result from the inhibition of  
559 corrosion in water.<sup>65</sup> The formation of nanocrystalline FeS phases on the surfaces of  
560 sulfidated NZVI, resulting in a high surface area and good electrical conductivity, has been  
561 suggested to be responsible for the high reactivity of these nanoparticles toward contaminants  
562 (Figure S6).<sup>128</sup> From a molecular point of view, dechlorination by reductive elimination may  
563 be favored over hydrogenolysis as a result of sulfidation.<sup>65</sup> In addition, the surface of  
564 sulfidated NZVI may act as a more efficient conductor of electrons from the inner Fe(0) to the  
565 surface layers than iron (oxyhydr)oxides.<sup>131,132</sup> Two recent review papers have highlighted  
566 progress made in this research area.<sup>65,133</sup>

567

## 568 **5.2. Depassivation during/after decontamination**

569 A significant amount of effort has been expended on the investigation of methods to  
570 extend the longevity of NZVI during the removal of environmental contaminants. For  
571 example, Bae and Lee<sup>8</sup> recently demonstrated that an endogenous electron shuttle (i.e.,



572 riboflavin) can enhance the long-term dechlorination of  $\text{CCl}_4$  by NZVI. Results from TEM  
573 surface analyses revealed the removal of the passivated layer (Figure S7), presumably due to  
574 reductive dissolution by riboflavin, which could result in an increase in the rate of electron  
575 transfer. In addition, Wang et al.<sup>14</sup> revealed that the addition of humic acid enhanced the rate  
576 and extent of 4-chlorobiphenyl degradation by NZVI, given that the humic acid acted as an  
577 electron shuttle, thus leading to the rapid transfer of electrons from NZVI to the contaminant.  
578 Although the investigators did not investigate the depassivation of NZVI,<sup>8,14</sup> their  
579 experimental results indicated that other electron shuttles such as quinone moieties (e.g., *p*-  
580 hydroquinone, lawsone, 9,10-anthraquinone-2,6-disulfonate (AQDS), etc.) may also lead to  
581 an increase in the longevity of NZVI.

582 Ultrasound has commonly been used to improve the dispersivity and stability of NZVI  
583 during decontamination of wastewater.<sup>134,135</sup> This process induces cavitation leading to  
584 extremely high local temperatures (up to 10000 K) and pressures (up to 5000 bar).<sup>136</sup> This can  
585 cause pitting and cracking at particle surfaces resulting in the removal of the passivated  
586 surface (oxyhydr)oxide layer.<sup>137</sup> The enhanced removal of several elements, including  $\text{Zn}^{2+}$ ,  
587  $\text{Pb}^{2+}$  and  $\text{Cu}^{2+}$  has been observed following the application of ultrasound with the increased  
588 removal due probably to the removal of the passivated layer.<sup>136</sup>

589 There have been very few studies on the regeneration of passivated NZVI after  
590 decontamination<sup>138</sup> although several studies have been conducted on ZVI.<sup>85,116,139</sup> Due to the  
591 different Fe (oxyhydr)oxides that may form on corrosion of NZVI and ZVI and the inherent  
592 physical and chemical differences of these particles, it is not appropriate to necessarily  
593 assume similar mechanistic processes are operative for ZVI and NZVI. For example, a  
594 significant enhancement of TCE reduction was observed when an iron reducing bacteria  
595 (*Shewanella putrefaciens*) was inoculated into a passivated ZVI suspension but not when  
596 introduced to NZVI.<sup>138</sup> It was speculated that the biologically-mediated reductive dissolution

597 of the passivating layer re-exposed the ZVI Fe(0) core whereas a minimal amount of Fe(0)  
598 was conserved in the case of passivated NZVI. Overall, the lack of studies on NZVI  
599 depassivation after decontamination reactions is a result of the small size and highly reactive  
600 nature of NZVI, which generally leads to its rapid transformation to Fe(II) and Fe(III)  
601 minerals.

602

## 603 **6. ENVIRONMENTAL SIGNIFICANCE AND FUTURE APPLICATIONS**

604 NZVI has been one of the most intensively studied nanomaterials in environmental  
605 engineering over the past 20 years, particularly in relation to its potential use in remediating  
606 soil, groundwater and wastewater. Despite the extensive *in situ* and *ex-situ* use of NZVI for  
607 contaminant removal, rapid surface passivation resulting in loss of NZVI reactivity is  
608 considered one of the most severe problems with regard to its effective application. As  
609 discussed in this review, the nature and extent of NZVI passivation may differ markedly  
610 depending on the particular conditions in which NZVI is applied (Figure 6). As such, the need  
611 exists to investigate the particular passivation mechanism, the factors that influence the rate  
612 and extent of passivation and possible depassivation techniques suited to promoting the  
613 efficacy of NZVI for each proposed application.

614 Most of the published literature to date has investigated the reactivity of NZVI with very  
615 little attention paid to its passivation mechanisms. The reaction between NZVI and  
616 contaminants is generally used to assess particle reactivity, however analyses of NZVI  
617 transformations have rarely been conducted by investigators. Moreover, passivation effects  
618 are more significant when NZVI is applied at a pilot- and/or field-scale due to the presence of  
619 many influencing factors (e.g., long reaction time, O<sub>2</sub> levels, presence of inorganic and  
620 organic contaminants and biotic influences). A systematic analysis of the effects of

621 passivation is therefore necessary to provide a comprehensive understanding of NZVI  
622 chemistry during long-term applications (e.g., groundwater and soil remediation).

623 In this review, the most recent information with respect to the characterization techniques  
624 for identifying passivation mechanisms have been summarized, in addition to important  
625 factors that influence depassivation under different O<sub>2</sub> conditions and thereby extend the  
626 longevity of NZVI. It becomes clear that there are significant challenges to overcome to  
627 further advance NZVI as a remedial agent for environmental pollution. These challenges  
628 include: (i) the establishment of advanced time-resolved methodologies to monitor NZVI  
629 transformations; (ii) the evaluation of the contribution of passivation byproducts to sequential  
630 contaminant removal; (iii) the investigation of microbial populations promoted by the  
631 passivation byproducts after soil and groundwater remediation and (iv) the development of  
632 novel and efficient depassivation strategies during and after NZVI application.

633 In engineered systems (such as wastewater treatment), the assessment of NZVI corrosion  
634 byproducts and depassivation ways in order to improve and/or maintain contaminant removal  
635 performance will be critical for developing a cost-effective NZVI-based technologies and  
636 designing large-scale applications. In natural systems (such as soil and groundwater  
637 environments) where nanoparticles are injected into affected zones, a comprehensive  
638 examination of the transformation and mobility of the injected nanoparticles is essential for  
639 ecological risk assessments. This will improve our ability to develop new simulation tools for  
640 accurately predicting the overall performance of NZVI-based technologies as well as the fate  
641 of NZVI particles in natural systems.

642

## 643 **ASSOCIATED CONTENT**

### 644 **Supporting Information**

645 The Supporting Information is available free of charge via on the ACS publications websites  
646 at DOI:

647 Figures S1 to S7 (PDF).

648

#### 649 **ACKNOWLEDGMENTS**

650 This research was partially supported by the framework of International Cooperation Program  
651 managed by National Research Foundation of Korea (NRF-2017K1A3A1A21013653) and  
652 Campus France (PHC STAR).

653

## 654 REFERENCES

- 655 (1) Alowitz, M. J.; Scherer, M. M., Kinetics of nitrate, nitrite, and Cr(VI) reduction by iron  
656 metal. *Environ. Sci. Technol.* **2002**, *36* (3), 299–306.
- 657 (2) Phillips, D. H.; Van Nooten, T.; Bastiaens, L.; Russell, M. I.; Dickson, K.; Plant, S.;  
658 Ahad, J. M. E.; Newton, T.; Elliot, T.; Kalin, R. M. Ten year performance evaluation of a  
659 field-scale zero-valent iron permeable reactive barrier installed to remediate  
660 trichloroethene contaminated groundwater. *Environ. Sci. Technol.* **2010**, *44* (10), 3861–  
661 3869.
- 662 (3) Bae, S.; Lee, W., Inhibition of nZVI reactivity by magnetite during the reductive  
663 degradation of 1,1,1-TCA in nZVI/magnetite suspension. *Appl. Catal. B-  
664 Environ.* **2010**, *96* (1–2), 10–17.
- 665 (4) Xie, Y.; Cwiertny, D. M., Influence of anionic cosolutes and pH on nanoscale zerovalent  
666 iron longevity: time scales and mechanisms of reactivity loss toward 1,1,1,2-  
667 tetrachloroethane and Cr(VI). *Environ. Sci. Technol.* **2012**, *46* (15), 8365–8373.
- 668 (5) Lowry, G. V.; Johnson, K. M., Congener-specific dechlorination of dissolved PCBs by  
669 microscale and nanoscale zerovalent iron in a water/methanol solution. *Environ. Sci.  
670 Technol.* **2004**, *38* (19), 5208–5216.
- 671 (6) Bae, S.; Hanna, K., Reactivity of nanoscale zero-valent iron in unbuffered systems: effect  
672 of pH and Fe(II) dissolution. *Environ. Sci. Technol.* **2015**, *49* (17), 10536–10543.
- 673 (7) Smith, K. S.; Huyck, H. L. O. An overview of the abundance, relative mobility,  
674 bioavailability, and human toxicity of metals. In *The Environmental Geochemistry of  
675 Mineral Deposits. Part A: Processes, Techniques, and Health Issues*; Plumlee, G.  
676 S.; Logsdon, M. J., Eds.; Society of Economic Geologists: Littleton, CO, **1999**; Vol. 6A.
- 677 (8) Bae, S.; Lee, W., Influence of riboflavin on nanoscale zero-valent iron reactivity during  
678 the degradation of carbon tetrachloride. *Environ. Sci. Technol.* **2014**, *48* (4), 2368–2376.
- 679 (9) Song, H.; Carraway, E. R. Reduction of chlorinated ethanes by nanosized zero-valent iron:  
680 kinetics, pathways, and effects of reaction conditions. *Environ. Sci. Technol.* **2005**, *39*,  
681 6237–6245.
- 682 (10) Wang, C. B.; Zhang, W. X. Synthesizing nanoscale iron particles for rapid and complete  
683 dechlorination of TCE and PCBs. *Environ. Sci. Technol.* **1997**, *31*, 2154–2156.
- 684 (11) Cheng, R.; Wang, J. L.; Zhang, W. X. Comparison of reductive dechlorination of p-  
685 chlorophenol using Fe<sup>0</sup> and nanosized Fe<sup>0</sup>. *J. Hazard. Mater.* **2007**, *144* (1–2), 334–339.
- 686 (12) Ryu, A.; Jeong, S. W.; Jang, A.; Choi, H., Reduction of highly concentrated nitrate using  
687 nanoscale zero-valent iron: Effects of aggregation and catalyst on reactivity. *Appl. Catal.  
688 B-Environ.* **2011**, *105* (1–2), 128–135.
- 689 (13) Shih, Y. H.; Hsu, C. Y.; Su, Y. F. Reduction of hexachlorobenzene by nanoscale zero-  
690 valent iron: Kinetics, pH effect, and degradation mechanism. *Sep. Purif.  
691 Tech.* **2011**, *76* (3), 268–274.
- 692 (14) Wang, Y.; Zhou, D. M.; Wang, Y. J.; Zhu, X. D.; Jin, S. Y. Humic acid and metal ions  
693 accelerating the dechlorination of 4-chlorobiphenyl by nanoscale zero-valent iron. *J.  
694 Environ. Sci-China* **2011**, *23* (8), 1286–1292.
- 695 (15) Chekli, L.; Bayatsarmadi, B.; Sekine, R.; Sarkar, B.; Shen, A. M.; Scheckel, K. G.;  
696 Skinner, W.; Naidu, R.; Shon, H. K.; Lombi, E.; Donner, E. Analytical characterisation of  
697 nanoscale zero-valent iron: A methodological review. *Anal. Chim. Acta* **2016**, *903*, 13–35.
- 698 (16) Giasuddin, A. B. M.; Kanel, S. R.; Choi, H. Adsorption of humic acid onto nanoscale  
699 zerovalent iron and its effect on arsenic removal. *Environ. Sci. Technol.* **2007**, *41* (6),  
700 2022–2027.

- 701 (17) Li, X. Q.; Cao, J. S.; Zhang, W. X. Stoichiometry of Cr(VI) immobilization using  
702 nanoscale zerovalent iron (nZVI): A study with high-resolution X-ray photoelectron  
703 spectroscopy (HR-XPS). *Ind. Eng. Chem. Res.* **2008**, *47* (7), 2131–2139.
- 704 (18) Dong, H. R.; Guan, X. H.; Lo, I. M. C. Fate of As(V)-treated nano zero-valent iron:  
705 Determination of arsenic desorption potential under varying environmental conditions by  
706 phosphate extraction. *Water Res.* **2012**, *46* (13), 4071–4080.
- 707 (19) Kanel, S. R.; Greneche, J. M.; Choi, H. Arsenic(V) removal from groundwater using  
708 nano scale zero-valent iron as a colloidal reactive barrier material. *Environ. Sci. Technol.*  
709 **2006**, *40* (6), 2045–2050.
- 710 (20) Kanel, S. R.; Nepal, D.; Manning, B.; Choi, H. Transport of surface-modified iron  
711 nanoparticle in porous media and application to arsenic(III) remediation. *J. Nanopart.*  
712 *Res.* **2007**, *9* (5), 725–735.
- 713 (21) Yan, W.; Vasic, R.; Frenkel, A. I.; Koel, B. E. Intraparticle reduction of arsenite (As(III))  
714 by nanoscale zerovalent iron (nZVI) investigated with in situ X-ray absorption  
715 spectroscopy. *Environ. Sci. Technol.* **2012**, *46* (13), 7018–7026.
- 716 (22) Kanel, S. R.; Manning, B.; Charlet, L.; Choi, H. Removal of arsenic(III) from  
717 groundwater by nanoscale zero-valent iron. *Environ. Sci. Technol.* **2005**, *39* (5), 1291–  
718 1298.
- 719 (23) Zhang, Y. L.; Li, Y. T.; Dai, C. M.; Zhou, X. F.; Zhang, W. X. Sequestration of Cd(II)  
720 with nanoscale zero-valent iron (nZVI): Characterization and test in a two-stage  
721 system. *Chem. Eng. J.* **2014**, *244*, 218–226.
- 722 (24) Tsarev, S.; Collins, R. N.; Ilton, E. S.; Fahy, A.; Waite, T. D. The short-term reduction of  
723 uranium by nanoscale zero-valent iron (nZVI): role of oxide shell, reduction mechanism  
724 and the formation of U(V)-carbonate phases. *Environ. Sci. Nano* **2017**, *4* (6), 1304–1313.
- 725 (25) Sihn, Y.; Bae, S.; Lee, W. Formation of surface mediated iron colloids during U(VI) and  
726 nZVI interaction, *Adv. Environ. Res.* **2013**, *2*, 167–177.
- 727 (26) Sheng, G. D.; Shao, X. Y.; Li, Y. M.; Li, J. F.; Dong, H. P.; Cheng, W.; Gao, X.; Huang,  
728 Y. Y. Enhanced removal of uranium(VI) by nanoscale zerovalent iron supported on Na-  
729 bentonite and an investigation of mechanism. *J. Phys. Chem. A* **2014**, *118* (16), 2952–  
730 2958.
- 731 (27) Fan, D. M.; Anitori, R. P.; Tebo, B. M.; Tratnyek, P. G.; Pacheco, J. S. L.; Kukkadapu, R.  
732 K.; Engelhard, M. H.; Bowden, M. E.; Kovarik, L.; Arey, B. W. Reductive sequestration  
733 of pertechnetate ( $^{99}\text{TcO}_4^-$ ) by nano zerovalent iron (nZVI) transformed by abiotic  
734 sulfide. *Environ. Sci. Technol.* **2013**, *47* (10), 5302–5310.
- 735 (28) Machado, S.; Stawinski, W.; Slonina, P.; Pinto, A. R.; Grosso, J. P.; Nouws, H. P. A.;  
736 Albergaria, J. T.; Delerue-Matos, C. Application of green zero-valent iron nanoparticles  
737 to the remediation of soils contaminated with ibuprofen. *Sci. Total. Environ.* **2013**, *461*,  
738 323–329.
- 739 (29) Karim, S.; Bae, S.; Greenwood, D.; Hanna, K.; Singhal, N. Degradation of 17 alpha-  
740 ethinylestradiol by nano zero valent iron under different pH and dissolved oxygen levels.  
741 *Water Res.* **2017**, *125*, 32–41.
- 742 (30) Joo, S. H.; Feitz, A. J.; Waite, T. D. Oxidative degradation of the carbothioate herbicide,  
743 molinate, using nanoscale zero-valent iron. *Environ. Sci. Technol.* **2004**, *38* (7), 2242–  
744 2247.
- 745 (31) Feitz, A. J.; Joo, S. H.; Guan, J.; Sun, Q.; Sedlak, D. L.; Waite, T. D. Oxidative  
746 transformation of contaminants using colloidal zero-valent iron. *Colloids Surf., A* **2005**,  
747 *265* (1–3), 88–94.

- 748 (32) Phenrat, T.; Saleh, N.; Sirk, K.; Tilton, R. D.; Lowry, G. V. Aggregation and  
749 sedimentation of aqueous nanoscale zerovalent iron dispersions. *Environ. Sci. Technol.*  
750 **2007**, *41* (1), 284–290.
- 751 (33) Reinsch, B. C.; Forsberg, B.; Penn, R. L.; Kim, C. S.; Lowry, G. V. Chemical  
752 transformations during aging of zerovalent iron nanoparticles in the presence of common  
753 groundwater dissolved constituents. *Environ. Sci. Technol.* **2010**, *44* (9), 3455–3461.
- 754 (34) Wang, F. F.; Wu, Y.; Gao, Y.; Li, H.; Chen, Z. L. Effect of humic acid, oxalate and  
755 phosphate on Fenton-like oxidation of microcystin-LR by nanoscale zero-valent iron. *Sep.*  
756 *Purif. Tech.* **2016**, *170*, 337–343.
- 757 (35) Fan, D. M.; Johnson, G. O.; Tratnyek, P. G.; Johnson, R. L. Sulfidation of nano  
758 zerovalent iron (nZVI) for improved selectivity during in-situ chemical reduction  
759 (ISCR). *Environ. Sci. Technol.* **2016**, *50* (17), 9558–9565.
- 760 (36) He, D.; Ma, J. X.; Collins, R. N.; Waite, T. D. Effect of structural transformation of  
761 nanoparticulate zero-valent iron on generation of reactive oxygen species. *Environ. Sci.*  
762 *Technol.* **2016**, *50* (7), 3820–3828.
- 763 (37) Ahn, J.; Kim, C.; Kim, H.; Hwang, K.; Hwang, I. Effects of oxidants on in situ treatment  
764 of a DNAPL source by nanoscale zero-valent iron: A field study. *Water Res.* **2016**, *107*,  
765 57–65.
- 766 (38) Liu, A. R.; Liu, J.; Pan, B. C.; Zhang, W. X. Formation of lepidocrocite ( $\gamma$ -FeOOH)  
767 from oxidation of nanoscale zero-valent iron (nZVI) in oxygenated water. *RSC*  
768 *Adv.* **2014**, *4* (101), 57377–57382.
- 769 (39) Filip, J.; Karlicky, F.; Marusak, Z.; Lazar, P.; Cernik, M.; Otyepka, M.; Zboril, R.  
770 Anaerobic reaction of nanoscale zerovalent iron with water: Mechanism and kinetics. *J.*  
771 *Phys. Chem. C* **2014**, *118* (25), 13817–13825.
- 772 (40) Jung, Y.; Choi, J.; Lee, W., Spectroscopic investigation of magnetite surface for the  
773 reduction of hexavalent chromium. *Chemosphere* **2007**, *68* (10), 1968–1975.
- 774 (41) Rashid, M.; Price, N. T.; Pinilla, M. A. G.; O'Shea, K. E. Effective removal of phosphate  
775 from aqueous solution using humic acid coated magnetite nanoparticles. *Water Res.*  
776 **2017**, *123*, 353–360.
- 777 (42) Bharath, G.; Alhseinat, E.; Ponpandian, N.; Khan, M. A.; Siddiqui, M. R.; Ahmed, F.;  
778 Alsharaeh, E. H. Development of adsorption and electrosorption techniques for removal  
779 of organic and inorganic pollutants from wastewater using novel magnetite/porous  
780 graphene-based nanocomposites. *Sep. Purif. Technol.* **2017**, *188*, 206–218.
- 781 (43) Shi, J.; Li, H. Y.; Lu, H. G.; Zhao, X. W. Use of carboxyl functional magnetite  
782 nanoparticles as potential sorbents for the removal of heavy metal ions from aqueous  
783 solution. *J. Chem. Eng. Data* **2015**, *60* (7), 2035–2041.
- 784 (44) Bae, S.; Joo, J. B.; Lee, W. Reductive dechlorination of carbon tetrachloride by  
785 bioreduction of nontronite. *J. Hazard. Mater.* **2017**, *334*, 104–111.
- 786 (45) Jeon, K.; Lee, N.; Bae, S.; Goddard, W. A.; Kim, H.; Lee, W. Theoretical and  
787 experimental studies of the dechlorination mechanism of carbon tetrachloride on a  
788 vivianite ferrous phosphate surface. *J. Phys. Chem. A* **2015**, *119* (22), 5714–5722.
- 789 (46) Bae, S.; Lee, W. Enhanced reductive degradation of carbon tetrachloride by biogenic  
790 vivianite and Fe(II). *Geochim. Cosmochim. Acta* **2012**, *85*, 170–186.
- 791 (47) Veeramani, H.; Alessi, D. S.; Suvorova, E. I.; Lezama-Pacheco, J. S.; Stubbs, J. E.; Sharp,  
792 J. O.; Dippon, U.; Kappler, A.; Bargar, J. R.; Bernier-Latmani, R. Products of abiotic  
793 U(VI) reduction by biogenic magnetite and vivianite. *Geochim. Cosmochim. Acta* **2011**,  
794 *75* (9), 2512–2528.

- 795 (48) Etique, M.; Zegeye, A.; Gregoire, B.; Carteret, C.; Ruby, C. Nitrate reduction by mixed  
796 iron(II-III) hydroxycarbonate green rust in the presence of phosphate anions: The key  
797 parameters influencing the ammonium selectivity. *Water Res.* **2014**, *48*, 29–39.
- 798 (49) Guerbois, D.; Ona-Nguema, G.; Morin, G.; Abdelmoula, M.; Laverman, A. M.; Mouchel,  
799 J. M.; Barthelemy, K.; Maillot, F.; Brest, J. Nitrite reduction by biogenic  
800 hydroxycarbonate green rusts: Evidence for hydroxy-nitrite green rust formation as an  
801 intermediate reaction product. *Environ. Sci. Technol.* **2014**, *48* (8), 4505–4514.
- 802 (50) Lee, W.; Batchelor, B. Abiotic, reductive dechlorination of chlorinated ethylenes by iron-  
803 bearing soil minerals. 2. Green rust. *Environ. Sci. Technol.* **2002**, *36* (24), 5348–5354.
- 804 (51) Orsetti, S.; Laskov, C.; Haderlein, S. B., Electron transfer between iron minerals and  
805 quinones: Estimating the reduction potential of the Fe(II)-goethite surface from AQDS  
806 speciation. *Environ. Sci. Technol.* **2013**, *47* (24), 14161–14168.
- 807 (52) Pecher, K.; Haderlein, S. B.; Schwarzenbach, R. P. Reduction of polyhalogenated  
808 methanes by surface-bound Fe(II) in aqueous suspensions of iron oxides. *Environ. Sci.*  
809 *Technol.* **2002**, *36* (8), 1734–1741.
- 810 (53) Jiang, W. J.; Pelaez, M.; Dionysiou, D. D.; Entezari, M. H.; Tsoutsou, D.; O'Shea, K.  
811 Chromium(VI) removal by maghemite nanoparticles. *Chem. Eng. J.* **2013**, *222*, 527–533.
- 812 (54) Liu, H. B.; Chen, T. H.; Frost, R. L. An overview of the role of goethite surfaces in the  
813 environment. *Chemosphere* **2014**, *103*, 1–11.
- 814 (55) Wang, S. S.; Gao, B.; Zimmerman, A. R.; Li, Y. C.; Ma, L.; Harris, W. G.; Migliaccio, K.  
815 W. Removal of arsenic by magnetic biochar prepared from pinewood and natural  
816 hematite. *Bioresour. Technol.* **2015**, *175*, 391–395.
- 817 (56) Zhang, Y.; Zhi, Y.; Liu, J.; Ghoshal, S. Sorption of perfluoroalkyl acids to fresh and aged  
818 nanoscale zerovalent iron particles. *Environ. Sci. Tech.* **2018**, *52*, 6300–6308.
- 819 (57) Wang, S.; Gao, B.; Li, Y.; Creamer, A. E.; He, F. Adsorptive removal of arsenate from  
820 aqueous solutions by biochar supported zero-valent iron nanocomposite: Batch and  
821 continuous flow tests. *J. Hazard. Mater.* **2017**, *322*, 172–181
- 822 (58) Phenrat, T.; Long, T. C.; Lowry, G. V.; Veronesi, B. Partial oxidation ("aging") and  
823 surface modification decrease the toxicity of nanosized zerovalent iron. *Environ. Sci.*  
824 *Technol.* **2009**, *43* (1), 195–200.
- 825 (59) Auffan, M.; Achouak, W.; Rose, J.; Roncato, M. A.; Chaneac, C.; Waite, D. T.; Masion,  
826 A.; Woicik, J. C.; Wiesner, M. R.; Bottero, J. Y. Relation between the redox state of iron-  
827 based nanoparticles and their cytotoxicity toward Escherichia coli. *Environ. Sci. Technol.*  
828 **2008**, *42* (17), 6730–6735.
- 829 (60) Yan, W. L.; Ramos, M. A. V.; Koel, B. E.; Zhang, W. X. As(III) sequestration by iron  
830 nanoparticles: Study of solid-phase redox transformations with X-ray photoelectron  
831 spectroscopy. *J. Phys. Chem. C* **2012**, *116* (9), 5303–5311.
- 832 (61) Johnson, R. L.; Nurmi, J. T.; O'Brien Johnson, G. S.; Fan, D.; O'Brien Johnson, R. L.;  
833 Shi, Z.; Salter-Blanc, A. J.; Tratnyek, P. G.; Lowry, G. V. Field-scale transport and  
834 transformation of carboxymethylcellulose-stabilized nano zero-valent iron. *Environ. Sci.*  
835 *Technol.* **2013**, *47*, 1573–1580.
- 836 (62) Kocur, C. M.; Chowdhury, A. I.; Sakulchaicharoen, N.; Boparai, H. K.; Weber, K. P.;  
837 Sharma, P.; Krol, M. M.; Austrins, L.; Peace, C.; Sleep, B. E.; O'Carroll, D. M.  
838 Characterization of nZVI mobility in a field scale test. *Environ. Sci. Technol.* **2014**, *48*,  
839 2862–2869.
- 840 (63) Del Bianco, L.; Fiorani, D.; Testa, A. M.; Bonetti, E.; Savini, L.; Signoretti, S.  
841 Magnetothermal behavior of a nanoscale Fe/Fe oxide granular system. *Phys. Rev.*  
842 *B* **2002**, *66* (17).



- 843 (64) Ezzatahmadi, N.; Ayoko, G. A.; Millar, G. J.; Speight, R.; Yan, C.; Li, J. H.; Li, S. Z.;  
844 Zhu, J. X.; Xi, Y. F. Clay-supported nanoscale zero-valent iron composite materials for  
845 the remediation of contaminated aqueous solutions: A review. *Chem. Eng. J.* **2017**, *312*,  
846 336–350.
- 847 (65) Fan, D. M.; Lan, Y.; Tratnyek, P. G.; Johnson, R. L.; Filip, J.; O'Carroll, D. M.; Garcia, A.  
848 N.; Agrawal, A. Sulfidation of iron-based materials: A review of processes and  
849 implications for water treatment and remediation. *Environ. Sci. Technol.* **2017**, *51* (22),  
850 13070–13085.
- 851 (66) Fu, F. L.; Dionysiou, D. D.; Liu, H. The use of zero-valent iron for groundwater  
852 remediation and wastewater treatment: A review. *J. Hazard. Mater.* **2014**, *267*, 194–205.
- 853 (67) Grafe, M.; Donner, E.; Collins, R. N.; Lombi, E. Speciation of metal(loid)s in  
854 environmental samples by X-ray absorption spectroscopy: A critical review. *Anal. Chim.*  
855 *Acta* **2014**, *822*, 1–22.
- 856 (68) Henderson, A. D.; Demond, A. H. Long-term performance of zero-valent iron permeable  
857 reactive barriers: A critical review. *Environ. Eng. Sci.* **2007**, *24* (4), 401–423.
- 858 (69) Li, L.; Fan, M. H.; Brown, R. C.; Van Leeuwen, J. H.; Wang, J. J.; Wang, W. H.; Song, Y.  
859 H.; Zhang, P. Y. Synthesis, properties, and environmental applications of nanoscale iron-  
860 based materials: A review. *Crit. Rev. Environ. Sci. Tech.* **2006**, *36* (5), 405–431.
- 861 (70) Mukherjee, R.; Kumar, R.; Sinha, A.; Lama, Y.; Saha, A. K. A review on synthesis,  
862 characterization, and applications of nano zero valent iron (nZVI) for environmental  
863 remediation. *Crit. Rev. Environ. Sci. Tech.* **2016**, *46* (5), 443–466.
- 864 (71) Raychoudhury, T.; Scheytt, T. Potential of zerovalent iron nanoparticles for remediation  
865 of environmental organic contaminants in water: a review. *Water Sci. Tech.* **2013**, *68* (7),  
866 1425–1439.
- 867 (72) Stefaniuk, M.; Oleszczuk, P.; Ok, Y. S. Review on nano zerovalent iron (nZVI): From  
868 synthesis to environmental applications. *Chem. Eng. J.* **2016**, *287*, 618–632.
- 869 (73) Tosco, T.; Papini, M. P.; Viggli, C. C.; Sethi, R. Nanoscale zerovalent iron particles for  
870 groundwater remediation: a review. *J. Clean. Prod.* **2014**, *77*, 10–21.
- 871 (74) Zou, Y. D.; Wang, X. X.; Khan, A.; Wang, P. Y.; Liu, Y. H.; Alsaedi, A.; Hayat, T.;  
872 Wang, X. K. Environmental remediation and application of nanoscale zero-valent iron  
873 and its composites for the removal of heavy metal ions: A review. *Environ. Sci. Technol.*  
874 **2016**, *50* (14), 7290–7304.
- 875 (75) Uzum, C.; Shahwan, T.; Eroglu, A. E.; Lieberwirth, I.; Scott, T. B.; Hallam, K. R.  
876 Application of zero-valent iron nanoparticles for the removal of aqueous  $\text{Co}^{2+}$  ions under  
877 various experimental conditions. *Chem. Eng. J.* **2008**, *144* (2), 213–220.
- 878 (76) Yan, W. L.; Herzing, A. A.; Li, X. Q.; Kiely, C. J.; Zhang, W. X. Structural evolution of  
879 Pd-doped nanoscale zero-valent iron (nZVI) in aqueous media and implications for  
880 particle aging and reactivity. *Environ. Sci. Technol.* **2010**, *44* (11), 4288–4294.
- 881 (77) Liu, A. R.; Liu, J.; Zhang, W. X. Transformation and composition evolution of nanoscale  
882 zero valent iron (nZVI) synthesized by borohydride reduction in static  
883 water. *Chemosphere* **2015**, *119*, 1068–1074.
- 884 (78) Liu, A.; Liu, J.; Han, J.; Zhang, W. X. Evolution of nanoscale zero-valent iron (nZVI) in  
885 water: Microscopic and spectroscopic evidence on the formation of nano- and micro-  
886 structured iron oxides. *J. Hazard. Mater.* **2017**, *322*, 129–135.
- 887 (79) Pullin, H.; Springell, R.; Parry, S.; Scott, T., The effect of aqueous corrosion on the  
888 structure and reactivity of zero-valent iron nanoparticles. *Chem. Eng. J.* **2017**, *308*, 568–  
889 577.

- 890 (80) Pullin, H.; Crane, R. A.; Morgan, D. J.; Scott, T. B. The effect of common groundwater  
891 anions on the aqueous corrosion of zero-valent iron nanoparticles and associated removal  
892 of aqueous copper and zinc. *J. Environ. Chem. Eng.* **2017**, *5* (1), 1166–1173.
- 893 (81) Schoftner, P.; Waldner, G.; Lottermoser, W.; Stoger-Pollach, M.; Freitag, P.;  
894 Reichenauer, T. G. Electron efficiency of nZVI does not change with variation of  
895 environmental parameters. *Sci. Total Environ.* **2015**, *535*, 69–78.
- 896 (82) Tsarev, S.; Collins, R. N.; Fahy, A.; Waite, T. D. Reduced uranium phases produced from  
897 anaerobic reaction with nanoscale zerovalent iron. *Environ. Sci. Technol.* **2016**, *50* (5),  
898 2595–2601.
- 899 (83) Hwang, Y.; Shin, H. S., Effects on nano zero-valent iron reactivity of interactions  
900 between hardness, alkalinity, and natural organic matter in reverse osmosis concentrate. *J.*  
901 *Environ. Sci-China* **2013**, *25* (11), 2177–2184.
- 902 (84) Wang, Q. L.; Kanel, S. R.; Park, H.; Ryu, A.; Choi, H. Controllable synthesis,  
903 characterization, and magnetic properties of nanoscale zerovalent iron with specific high  
904 Brunauer-Emmett-Teller surface area. *J. Nanopart. Res.* **2009**, *11* (3), 749–755.
- 905 (85) Liu, T. X.; Li, X. M.; Waite, T. D. Depassivation of aged Fe<sup>0</sup> by divalent cations:  
906 Correlation between contaminant degradation and surface complexation  
907 constants. *Environ. Sci. Technol.* **2014**, *48* (24), 14564–14571.
- 908 (86) Kim, H. S.; Ahn, J. Y.; Hwang, K. Y.; Kim, I. K.; Hwang, I. Atmospherically stable  
909 nanoscale zero-valent iron particles formed under controlled air contact: Characteristics  
910 and reactivity. *Environ. Sci. Technol.* **2010**, *44* (5), 1760–1766.
- 911 (87) Klimkova, S.; Cernik, M.; Lacinova, L.; Filip, J.; Jancik, D.; Zboril, R. Zero-valent iron  
912 nanoparticles in treatment of acid mine water from in situ uranium  
913 leaching. *Chemosphere* **2011**, *82* (8), 1178–1184.
- 914 (88) Ma, X. M.; He, D.; Jones, A. M.; Collins, R. N.; Waite, T. D. Reductive reactivity of  
915 borohydride- and dithionite-synthesized iron-based nanoparticles: A comparative study. *J.*  
916 *Hazard. Mater.* **2016**, *303*, 101–110.
- 917 (89) Sun, Y. P.; Li, X. Q.; Cao, J. S.; Zhang, W. X.; Wang, H. P. Characterization of zero-  
918 valent iron nanoparticles. *Adv. Colloid Interface Sci.* **2006**, *120* (1–3), 47–56.
- 919 (90) Lin, K. S.; Chang, N. B.; Chuang, T. D. Fine structure characterization of zero-valent iron  
920 nanoparticles for decontamination of nitrites and nitrates in wastewater and  
921 groundwater. *Sci. Tech. Adv. Mater.* **2008**, *9* (2).
- 922 (91) Wu, C.; Tu, J. W.; Liu, W. Z.; Zhang, J.; Chu, S. Q.; Lu, G. N.; Lin, Z.; Dang, Z. The  
923 double influence mechanism of pH on arsenic removal by nano zero valent iron:  
924 electrostatic interactions and the corrosion of Fe<sup>0</sup>. *Environ. Sci. Nano* **2017**, *4* (7), 1544–  
925 1552.
- 926 (92) Ma, J. X.; He, D.; Collins, R. N.; He, C. S.; Waite, T. D. The tortoise versus the hare -  
927 Possible advantages of microparticulate zerovalent iron (mZVI) over nanoparticulate  
928 zerovalent iron (nZVI) in aerobic degradation of contaminants. *Water Res.* **2016**, *105*,  
929 331–340.
- 930 (93) Ravel, B.; Newville, M., ATHENA, ARTEMIS, HEPHAESTUS: data analysis for X-ray  
931 absorption spectroscopy using IFEFFIT. *J. Synchrotron Rad.* **2005**, *12*, 537–541.
- 932 (94) Reardon, E. J.; Fagan, R.; Vogan, J. L.; Przepiora, A. Anaerobic corrosion reaction  
933 kinetics of nanosized iron. *Environ. Sci. Technol.* **2008**, *42* (7), 2420–2425.
- 934 (95) Zhang, L. N.; Zhou, M. F.; Shao, L. M.; Wang, W. N.; Fan, K. N.; Qin, Q. Z., Reactions  
935 of Fe with H<sub>2</sub>O and FeO with H<sub>2</sub>. A combined matrix isolation FTIR and theoretical  
936 study. *J. Phys. Chem. A* **2001**, *105* (29), 6998–7003.
- 937 (96) Linderoth, S.; Morup, S.; Bentzon, M. D. Oxidation of nanometer-sized iron particles. *J.*  
938 *Mater. Sci.* **1995**, *30*, 3142–3148.

- 939 (97) Cabrera, N.; Mott, N. F. Theory of the oxidation of metals. *Rep. Prog. Phys.* **1949**, *12*,  
940 163–184.
- 941 (98) Chernavskii, P. A.; Peskov, N. V.; Mugtasimov, A. V.; Lunin, V. V. Oxidation of metal  
942 nanoparticles: Experiment and model. *Russ. J. Phys. Chem. B* **2007**, *1* (4), 394–411.
- 943 (99) Roosendaal, S. J.; Bakker, J. P. R.; Vredenberg, A. M.; Habraken, F. H. P. M. Passivation  
944 of iron oxidation in H<sub>2</sub>O and O<sub>2</sub>/H<sub>2</sub>O mixtures. *Surf. Sci.* **2001**, *494* (3), 197–205.
- 945 (100) Grosvenor, A. P.; Kobe, B. A.; McIntyre, N. S. Studies of the oxidation of iron by air  
946 after being exposed to water vapour using angle-resolved X-ray photoelectron  
947 spectroscopy and QUASES. *Surf. Interface Anal.* **2004**, *36* (13), 1637–1641.
- 948 (101) Grosvenor, A. P.; Kobe, B. A.; McIntyre, N. S. Activation energies for the oxidation  
949 of iron by oxygen gas and water vapour. *Surf. Sci.* **2005**, *574* (2–3), 317–321.
- 950 (102) Sarathy, V.; Tratnyek, P. G.; Nurmi, J. T.; Baer, D. R.; Amonette, J. E.; Chun, C.;  
951 Penn, R. L.; Reardon, E. J. Aging of iron nanoparticles in aqueous solution: effects on  
952 structure and reactivity. *J. Phys. Chem. C* **2008**, *112*, 2286–2293.
- 953 (103) Greenlee, L. F.; Torrey, J. D.; Amaro, R. L.; Shaw, J. M. Kinetics of zero valent iron  
954 nanoparticle oxidation in oxygenated water. *Environ. Sci. Technol.* **2012**, *46* (23), 12913–  
955 12920.
- 956 (104) Dong, H.; Zhao, F.; Zeng, G. M.; Tang, L.; Fan, C. Z.; Zhang, L. H.; Zeng, Y. L.; He,  
957 Q.; Xie, Y. K.; Wu, Y. A. Aging study on carboxymethyl cellulose-coated zero-valent  
958 iron nanoparticles in water: Chemical transformation and structural evolution. *J. Hazard.  
959 Mater.* **2016**, *312*, 234–242.
- 960 (105) Dong, H.; Zhao, F.; He, Q.; Xie, Y. K.; Zeng, Y. L.; Zhang, L. H.; Tang, L.; Zeng, G.  
961 M. Physicochemical transformation of carboxymethyl cellulose-coated zero-valent iron  
962 nanoparticles (nZVI) in simulated groundwater under anaerobic conditions. *Sep. Purif.  
963 Tech.* **2017**, *175*, 376–383.
- 964 (106) Dong, H.; Jiang, Z.; Deng, J. M.; Zhang, C.; Cheng, Y. J.; Hou, K. J.; Zhang, L. H.;  
965 Tang, L.; Zeng, G. M. Physicochemical transformation of Fe/Ni bimetallic nanoparticles  
966 during aging in simulated groundwater and the consequent effect on contaminant  
967 removal. *Water Res.* **2018**, *129*, 51–57.
- 968 (107) Nurmi, J. T.; Tratnyek, P. G.; Sarathy, V.; Baer, D. R.; Amonette, J. E.; Pecher, K.;  
969 Wang, C. M.; Linehan, J. C.; Matson, D. W.; Penn, R. L.; Driessen, M. D.  
970 Characterization and properties of metallic iron nanoparticles: Spectroscopy,  
971 electrochemistry, and kinetics. *Environ. Sci. Technol.* **2005**, *39* (5), 1221–1230.
- 972 (108) Liu, Y.; Phenrat, T.; Lowry, G. V. Effect of TCE concentration and dissolved  
973 groundwater solutes on NZVI-Promoted TCE dechlorination and H<sub>2</sub> evolution. *Environ.  
974 Sci. Technol.* **2007**, *41* (22), 7881–7887.
- 975 (109) Su, Y. F.; Hsu, C. Y.; Shih, Y. H. Effects of various ions on the dechlorination kinetics  
976 of hexachlorobenzene by nanoscale zero-valent iron. *Chemosphere* **2012**, *88* (11), 1346–  
977 1352.
- 978 (110) Shih, Y. H.; Chen, M. Y.; Su, Y. F. Pentachlorophenol reduction by Pd/Fe bimetallic  
979 nanoparticles: Effects of copper, nickel, and ferric cations. *Appl. Catal. B-  
980 Environ.* **2011**, *105* (1–2), 24–29.
- 981 (111) Fan, J.; Guo, Y. H.; Wang, J. J.; Fan, M. H. Rapid decolorization of azo dye methyl  
982 orange in aqueous solution by nanoscale zerovalent iron particles. *J. Hazard. Mater.*  
983 **2009**, *166* (2–3), 904–910.
- 984 (112) Su, C. M.; Puls, R. W. Nitrate reduction by zerovalent iron: Effects of formate, oxalate,  
985 citrate, chloride, sulfate, borate, and phosphate. *Environ. Sci. Technol.* **2004**, *38* (9),  
986 2715–2720.

- 987 (113) Karabelli, D.; Uzum, C.; Shahwan, T.; Eroglu, A. E.; Scott, T. B.; Hallam, K. R.;  
988 Lieberwirth, I. Batch removal of aqueous  $\text{Cu}^{2+}$  ions using nanoparticles of zero-valent  
989 iron: A study of the capacity and mechanism of uptake. *Ind. Eng. Chem. Res.* **2008**, *47*  
990 (14), 4758–4764.
- 991 (114) Efecan, N.; Shahwan, T.; Eroglu, A. E.; Lieberwirth, I. Characterization of the uptake  
992 of aqueous  $\text{Ni}^{2+}$  ions on nanoparticles of zero-valent iron (nZVI). *Desalination* **2009**, *249*  
993 (3), 1048–1054.
- 994 (115) Zhang, Y. L.; Chen, W.; Dai, C. M.; Zhou, C. L.; Zhou, X. F. Structural evolution of  
995 nanoscale zero-valent iron (nZVI) in anoxic  $\text{Co}^{2+}$  solution: Interactional performance and  
996 mechanism. *Sci. Rep.* **2015**, *5*.
- 997 (116) Liu, T. X.; Li, X. M.; Waite, T. D. Depassivation of aged  $\text{Fe}^0$  by ferrous ions:  
998 Implications to contaminant degradation. *Environ. Sci. Technol.* **2013**, *47* (23), 13712–  
999 13720.
- 1000 (117) Kim, H-S.; Ahn, J-Y.; Kim, C.; Lee, S.; Hwang, I. Effect of anions and humic acid on  
1001 the performance of nanoscale zero-valent iron particles coated with polyacrylic acid.  
1002 *Chemosphere* **2014**, *113*, 93–100.
- 1003 (118) Glavee, G. N.; Klabunde, K. J.; Sorensen, C. M.; Hadjipanayis, G. C. Chemistry of  
1004 borohydride reduction of iron(II) and iron-(III) ions in aqueous and nonaqueous media -  
1005 formation of nanoscale Fe, FeB, and  $\text{Fe}_2\text{B}$  powders. *Inorg. Chem.* **1995**, *34*, 28–35.
- 1006 (119) McCormick, M. L.; Adriaens, P. Carbon tetrachloride transformation on the surface of  
1007 nanoscale biogenic magnetite particles. *Environ. Sci. Technol.* **2004**, *38*, 1045–1053.
- 1008 (120) Carpenter, E. E.; Calvin, S.; Stroud, R. M.; Harris, V. G. Passivated iron as core-shell  
1009 nanoparticles. *Chem. Mater.* **2003**, *15*, 3245–3246.
- 1010 (121) Bae, S.; Gim, S.; Kim, H.; Hanna, K. Effect of  $\text{NaBH}_4$  on properties of nanoscale  
1011 zero-valent iron and its catalytic activity for reduction of p-nitrophenol. *Appl. Catal. B:*  
1012 *Environ.* **2016**, *182*, 541–549.
- 1013 (122) Hua, Q.; Huang, W. Chemical etching induced shape change of magnetite  
1014 microcrystals. *J. Mater. Chem.* **2008**, *18*, 4286–4290.
- 1015 (123) Dong, H. R.; Lo, I. M. C. Influence of humic acid on the colloidal stability of surface-  
1016 modified nano zero-valent iron. *Water Res.* **2013**, *47* (1), 419–427.
- 1017 (124) Hydutsky, B. W.; Mack, E. J.; Beckerman, B. B.; Skluzacek, J. M.; Mallouk, T. E.  
1018 Optimization of nano- and microiron transport through sand columns using  
1019 polyelectrolyte mixtures. *Environ. Sci. Technol.* **2007**, *41* (18), 6418–6424.
- 1020 (125) Lee, C.; Keenan, C. R.; Sedlak, D. L. Polyoxometalate-enhanced oxidation of organic  
1021 compounds by nanoparticulate zero-valent iron and ferrous ion in the presence of oxygen.  
1022 *Environ. Sci. Technol.* **2008**, *42* (13), 4921–4926.
- 1023 (126) Kim, H. H.; Lee, H.; Kim, H. E.; Seo, J.; Hong, S. W.; Lee, J. Y.; Lee, C.  
1024 Polyphosphate-enhanced production of reactive oxidants by nanoparticulate zero-valent  
1025 iron and ferrous ion in the presence of oxygen: Yield and nature of oxidants. *Water Res.*  
1026 **2015**, *86*, 66–73.
- 1027 (127) Keenan, C. R.; Sedlak, D. L. Ligand-enhanced reactive oxidant generation by  
1028 nanoparticulate zero-valent iron and oxygen. *Environ. Sci. Technol.* **2008**, *42* (18), 6936–  
1029 6941.
- 1030 (128) Kim, E. J.; Kim, J. H.; Azad, A. M.; Chang, Y. S. Facile Synthesis and  
1031 Characterization of Fe/FeS Nanoparticles for Environmental Applications. *ACS Appl.*  
1032 *Mater. Inter.* **2011**, *3* (5), 1457–1462.
- 1033 (129) Scott, T. B.; Dickinson, M.; Crane, R. A.; Riba, O.; Hughes, G. M.; Allen, G. C. The  
1034 effects of vacuum annealing on the structure and surface chemistry of iron  
1035 nanoparticles. *J. Nanopart. Res.* **2010**, *12* (5), 1765–1775.

- 1036 (130) Riba, O.; Barnes, R. J.; Scott, T. B.; Gardner, M. N.; Jackman, S. A.; Thompson, I. P.  
1037 Enhanced reactivity of nanoscale iron particles through a vacuum annealing process. *J.*  
1038 *Nanopart. Res.* **2011**, *13* (10), 4591–4601.
- 1039 (131) Gong, Y. Y.; Gai, L. S.; Tang, J. C.; Fu, J.; Wang, Q. L.; Zeng, E. Y. Reduction of  
1040 Cr(VI) in simulated groundwater by FeS-coated iron magnetic nanoparticles. *Sci. Total.*  
1041 *Environ.* **2017**, *595*, 743–751.
- 1042 (132) Cao, Z.; Liu, X.; Xu, J.; Zhang, J.; Yang, Y.; Zhou, J. L.; Xu, X. H.; Lowry, G. V.  
1043 Removal of antibiotic florfenicol by sulfide-modified nanoscale zero-valent iron.  
1044 *Environ. Sci. Technol.* **2017**, *51* (19), 11269–11277.
- 1045 (133) Li, J.; Zhang, X.; Sun, Y.; Liang, L.; Pan, B.; Zhang, W.; Guan, X. Advances in  
1046 sulfidation of zerovalent iron for water decontamination. *Environ. Sci. Technol.*  
1047 **2017**, *51* (23), 13533–13544.
- 1048 (134) Liang, F.; Fan, J.; Guo, Y. H.; Fan, M. H.; Wang, J. J.; Yang, H. Q. Reduction of  
1049 nitrite by ultrasound-dispersed nanoscale zero-valent iron particles. *Ind. Eng. Chem. Res.*  
1050 **2008**, *47* (22), 8550–8554.
- 1051 (135) Rasheed, Q. J.; Pandian, K.; Muthukumar, K., Treatment of petroleum refinery  
1052 wastewater by ultrasound-dispersed nanoscale zero-valent iron particles. *Ultrason.*  
1053 *Sonochem.* **2011**, *18* (5), 1138–1142.
- 1054 (136) Mikhailov, I.; Mandal, A. R.; Kotov, S.; Kuznetsov, D. A new ultrasound-assisted  
1055 method of wastewater treatment by air-stable nanosized zero-valent iron. *Adv.*  
1056 *Electrochem.* **2014**, *1*, 1–4.
- 1057 (137) Geiger, C. L.; Ruiz, N. E.; Clausen, C. A.; Reinhart, D. R.; Quinn, J. W. Ultrasound  
1058 pretreatment of elemental iron: kinetic studies of dehalogenation reaction enhancement  
1059 and surface effects. *Water Res.* **2002**, *36* (5), 1342–1350.
- 1060 (138) Yang, Z. L.; Wang, X. L.; Li, H.; Yang, J.; Zhou, L. Y.; Liu, Y. D. Re-activation of  
1061 aged-ZVI by iron-reducing bacterium *Shewanella putrefaciens* for enhanced reductive  
1062 dechlorination of trichloroethylene. *J. Chem. Technol. Biot.* **2017**, *92* (10), 2642–2649.
- 1063 (139) Lu, X.; Li, M.; Tang, C.; Feng, C.; Liu, X. Electrochemical depassivation for  
1064 recovering Fe<sup>0</sup> reactivity by Cr(VI) removal with a permeable reactive barrier system. *J.*  
1065 *Hazard. Mater.* **2012**, 213–214, 355–360.
- 1066 (140) Liu, Y.; Lowry, G. V. Effect of particle age (Fe<sup>0</sup> content) and solution pH on NZVI  
1067 reactivity: H<sub>2</sub> evolution and TCE dichlorination. *Environ. Sci. Technol.* **2006**, *40*, 6085–  
1068 6090.

**Table 1. Representative studies reporting passivation byproducts of NZVI under different experimental conditions.**

Synthesis method	Reaction condition	O <sub>2</sub> condition	Reaction time	Passivation byproduct	Refs
Fe <sup>3+</sup> + NaBH <sub>4</sub>	complete mixing	oxygenated water + oxic condition	3 d	Lepi	38
FeCl <sub>3</sub> ·6H <sub>2</sub> O + NaBH <sub>4</sub>	no mixing	oxygenated water	5 d	Magn/Magh	77
		+ oxic condition	10 d	Ferr/ Magn/Magh	
			90 d	Lepi	
Fe <sub>2</sub> (SO <sub>4</sub> ) <sub>3</sub> ·6H <sub>2</sub> O + NaBH <sub>4</sub>	Cl <sup>-</sup> (10 mM)	water	2 h	Magn/Magh	80
		+ oxic condition	2 w	Akag/ Magn/Magh	
			16 w	Lepi /Magn/Magh	
Fe <sub>2</sub> (SO <sub>4</sub> ) <sub>3</sub> ·6H <sub>2</sub> O + NaBH <sub>4</sub>	HCO <sub>3</sub> <sup>-</sup> (10 mM)	water	2 h	Magn/Magh	80
		+ oxic condition	8 w	Goet/ Magn/Magh	
Fe <sub>2</sub> (SO <sub>4</sub> ) <sub>3</sub> ·6H <sub>2</sub> O + NaBH <sub>4</sub>	NO <sub>3</sub> <sup>-</sup> (10 mM)	water	2 h	Magn/Magh	80
		+ oxic condition	16 h	Magn/Magh	
Fe <sub>2</sub> (SO <sub>4</sub> ) <sub>3</sub> ·6H <sub>2</sub> O + NaBH <sub>4</sub>	SO <sub>4</sub> <sup>2-</sup> (10 mM)	water	2 h	Magn/Magh	80
		+ oxic condition	2 w	Lepi/Magn/Magh	
			16 w	Goet/Lepi/Magn/Magh	

RNIP 10-DP, product from Toda Kogyo Corp., Reduction of Fe(III) oxides by H <sub>2</sub>	NO <sub>3</sub> <sup>-</sup> (10 mM) + rotated end-over-end at 22 °C	deaerated water + anoxic condition	6 m	Magn	33
RNIP 10-DP, product from Toda Kogyo Corp., Reduction of Fe(III) oxides by H <sub>2</sub>	PO <sub>4</sub> <sup>2-</sup> (10 mM) + rotated end-over-end at 22 °C	deaerated water + anoxic condition	1 m 6 m	Magn Vivi/Schw	33
NANOFER 25DS, product from NANO IRON (inorganic S based coating), Reduction of Fe(III) oxides by H <sub>2</sub>	Synthetic groundwater (Cl <sup>-</sup> (1.95 mN), HCO <sub>3</sub> <sup>-</sup> (1.14 mN), NO <sub>3</sub> <sup>-</sup> (0.15 mN), SO <sub>4</sub> <sup>2-</sup> (0.44 mM))	deaerated water + anoxic condition		Magn	117
NANOFER 25 DS, product from NANO IRON (inorganic S based coating), Reduction of Fe(III) oxides by H <sub>2</sub>	Synthetic groundwater (Cl <sup>-</sup> (1.95 mN), HCO <sub>3</sub> <sup>-</sup> (1.14 mN), NO <sub>3</sub> <sup>-</sup> (0.15 mN), SO <sub>4</sub> <sup>2-</sup> (0.44 mM)) + Humic acid (2.5 mg L <sup>-1</sup> )	deaerated water + anoxic condition		Iron carbonate hydroxide hydrate	117
FeCl <sub>3</sub> •6H <sub>2</sub> O + NaBH <sub>4</sub>	microcystin-LR (5.0 mg L <sup>-1</sup> ) + PO <sub>4</sub> <sup>2-</sup> (0.4 mM) + added H <sub>2</sub> O <sub>2</sub> (6.6 mM)	water + oxic condition	4 h	Vivi	34
FeCl <sub>3</sub> •6H <sub>2</sub> O + NaBH <sub>4</sub>	microcystin-LR (5.0 mg L <sup>-1</sup> ) + humic acid (0.4 mM) + added H <sub>2</sub> O <sub>2</sub> (6.6 mM)	water + oxic condition	4 h	Lepi	34

$\text{FeCl}_3 \cdot 6\text{H}_2\text{O} + \text{NaBH}_4$	microcystin-LR ( $5.0 \text{ mg L}^{-1}$ ) + oxalate ( $0.4 \text{ mM}$ ) + added $\text{H}_2\text{O}_2$ ( $6.6 \text{ mM}$ )	water + oxic condition	4 h	Magn/Lepi	34
NANOFER STAR, product from NANO IRON	synthetic groundwater with an ionic strength of $15 \text{ mM}$	groundwater + anoxic condition	6 d	Amak/Goet/Magn	81
$\text{Fe}^{3+} + \text{NaBH}_4$	As(V) ( $2 \text{ mg L}^{-1}$ ) + synthetic groundwater at pH 5	groundwater + oxic condition	30 d 60 d	Magn/Magh/Lepi/Hema Lepi	18
$\text{Fe}^{3+} + \text{NaBH}_4$	synthetic groundwater at pH 9	groundwater 1 IU+ oxic condition	30 d 60 d	Magn/Magh Magn/Magh	18
$\text{FeSO}_4 \cdot 7\text{H}_2\text{O} + \text{NaBH}_4$	U(VI):Fe(0)=1:21, $50 \text{ mM NaCl}$ , $5.8 \text{ mM NaHCO}_3$ and $1 \text{ mM CaCl}_2$ , synthetic groundwater at pH 7	groundwater + anoxic condition	3 d 12 m	Chuk Chuk/Magn	82
$\text{FeCl}_3 \cdot 6\text{H}_2\text{O} + \text{NaBH}_4$	$\text{NO}_3^-$ ( $100 \text{ mg L}^{-1}$ ), $\text{HCO}_3^-$ ( $5 \text{ g L}^{-1}$ )	deaerated water + anoxic condition	3 h	Gree( $\text{CO}_3$ )	83
$\text{FeCl}_3 \cdot 6\text{H}_2\text{O} + \text{NaBH}_4$	$\text{NO}_3^-$ ( $100 \text{ mg L}^{-1}$ ), Humic acid ( $1 \text{ g L}^{-1}$ ; DOC = $320 \text{ mg L}^{-1}$ )	deaerated water + anoxic condition	3 h	Magn	83
$\text{FeCl}_3 \cdot 6\text{H}_2\text{O} + \text{NaBH}_4$	complete mixing at 300 rpm	deaerated water + anoxic condition	3 d	Wust/Goet/Lepi	78



FeSO <sub>4</sub> •7H <sub>2</sub> O + NaBH <sub>4</sub> + carboxymethyl cellulose	Na <sub>2</sub> S <sub>2</sub> O <sub>4</sub> (0.1 M), rolling on a hematology mixer at 15 rpm and pH 7.2	deaerated water + anoxic condition	2 d	Mack	35
FeCl <sub>2</sub> •4H <sub>2</sub> O + NaBH <sub>4</sub>	1 μM H <sup>14</sup> COO <sup>-</sup> , pH 6.2–8.3	oxygenated water + oxic condition	1 d	Side	36
RNIP 10-DS, product from Toda America, Inc. Reduction of Fe(III) oxides by H <sub>2</sub>	Dry powder	deaerated water + anoxic condition	<20 d	Mixed-valent Fe(II) and Fe(III) oxide	102
RNIP 10-DP, product from Toda Kogyo Corp. Reduction of Fe(III) oxides by H <sub>2</sub>	Alkaline slurry, pH =10.6	deaerated water + anoxic	2 y	Magn	140

Lepi: Lepidocrocite ( $\gamma$ -Fe<sup>III</sup>OOH), Magn: Magnetite ( $\text{Fe}^{\text{II}}\text{Fe}^{\text{III}}_2\text{O}_4$ ), Magh: Maghemite ( $\gamma$ -Fe<sup>III</sup><sub>2</sub>O<sub>3</sub>), Ferr: Ferrihydrite ( $5\text{Fe}^{\text{III}}_2\text{O}_3 \cdot 9\text{H}_2\text{O}$ ), Akag: akageneite ( $\beta$ -Fe<sup>III</sup>OOH), Schw: schwertmannite ( $\text{Fe}^{\text{III}}_{16}\text{O}_{16}(\text{OH},\text{SO}_4)_{12-13} \cdot 10-12\text{H}_2\text{O}$ ), Wust: wüstite (Fe<sup>II</sup>O), Amak: amakinite (Fe<sup>II</sup>(OH)<sub>2</sub>), Goet: goethite ( $\alpha$ -Fe<sup>III</sup>OOH), Hema: hematite ( $\alpha$ -Fe<sup>III</sup><sub>2</sub>O<sub>3</sub>), Vivi: vivianite (Fe<sup>II</sup><sub>3</sub>(PO<sub>4</sub>)<sub>2</sub>•8H<sub>2</sub>O), Gree(CO<sub>3</sub>): Carbonate green rust: [Fe<sup>II</sup><sub>4</sub>Fe<sup>III</sup><sub>2</sub>(OH)<sub>12</sub>][CO<sub>2</sub>•H<sub>2</sub>O], Mack: mackinawite (Fe<sup>II</sup>S), Side: siderite (Fe<sup>II</sup>CO<sub>3</sub>)

**Figure captions**

Figure 1. STEM images and XEDS maps showing NZVI oxidation by oxygen-containing water (a) fresh NZVI, (b) after 30 min and (c) 5 h reaction. (d) The corresponding graph shows the proportions of Fe present as either Fe(0), ferrihydrite or lepidocrocite as determined by linear combination fitting of EXAFS data. Reproduced with permission from ref 36, Copyright 2016, American Chemical Society.

Figure 2. TEM images of NZVI after reaction with water under anoxic conditions at (a) 25 and (b) 80 °C, respectively, and the long-term corrosion results at (c) 25 and (d) 80 °C, showing the proportions of Fe present as either Fe(0), Fe(OH)<sub>2</sub>, or magnetite as determined by <sup>57</sup>Fe Mössbauer Spectroscopy. Reproduced with permission from ref 39, Copyright 2014, American Chemical Society.

Figure 3. A conceptual model on the passivation of NZVI in water showing that the main passivation byproducts include wustite (FeO), goethite ( $\alpha$ -FeOOH) and akaganeite ( $\beta$ -FeOOH) under anoxic conditions while crystalline lepidocrocite ( $\gamma$ -FeOOH) with acicular-shaped structures forms under oxic conditions. Reproduced with permission from ref 78, Copyright 2017, Elsevier.

Figure 4. Results of TEM (a and c) and XRD (b and d) of NZVI showing the passivation of NZVI over one month at pH 8 in 5 and 25 mM HCO<sub>3</sub><sup>-</sup> suspensions. The XRD diffraction patterns associated with specific mineral phases are noted as  $\alpha$ -Fe for Fe(0), M for magnetite, GR for carbonate green rust, and ICH for iron carbonate hydroxide. Reproduced with permission from ref 4, Copyright 2012, American Chemical Society.

Figure 5. Schematic illustration showing the cation-induced depassivation process of aged micro-scale ZVI by Fe(II) dissolution of sheet or shell structures upon metal complexation on the NZVI surface. Cations:  $M^{2+}$ :  $Ba^{2+}$ ,  $Sr^{2+}$ ,  $Ca^{2+}$ ,  $Mg^{2+}$ ,  $Mn^{2+}$ ,  $Co^{2+}$ ,  $Fe^{2+}$ ,  $Ni^{2+}$ ,  $Zn^{2+}$ ,  $Pb^{2+}$ , and  $Cu^{2+}$ . Reproduced with permission from ref 85, Copyright 2014, American Chemical Society.

Figure 6. Schematic illustrations showing the NZVI applications, typical passivation process of NZVI at different conditions, and environmental significance of the passivation.

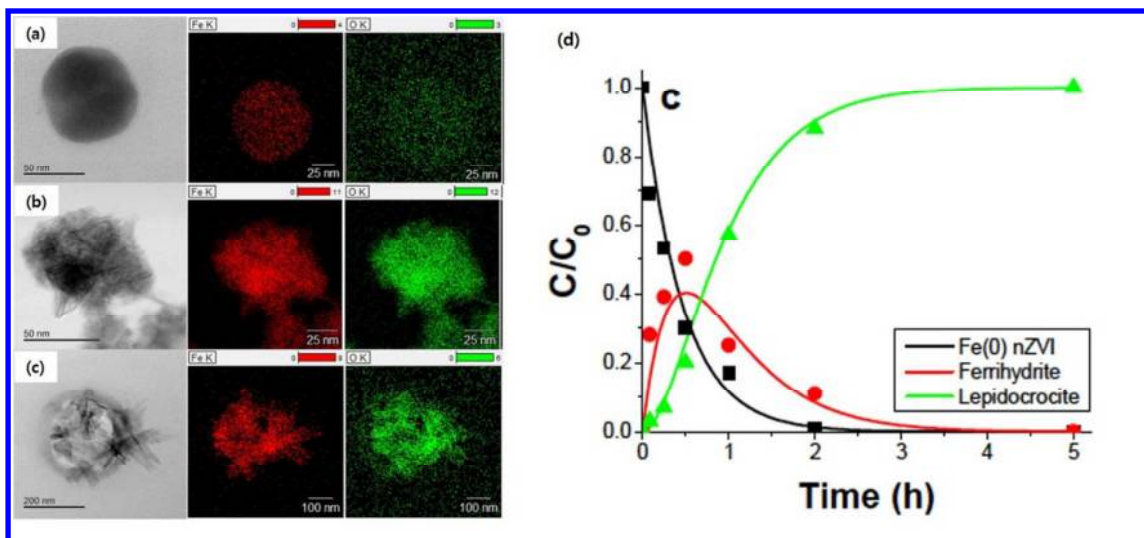


Figure 1.

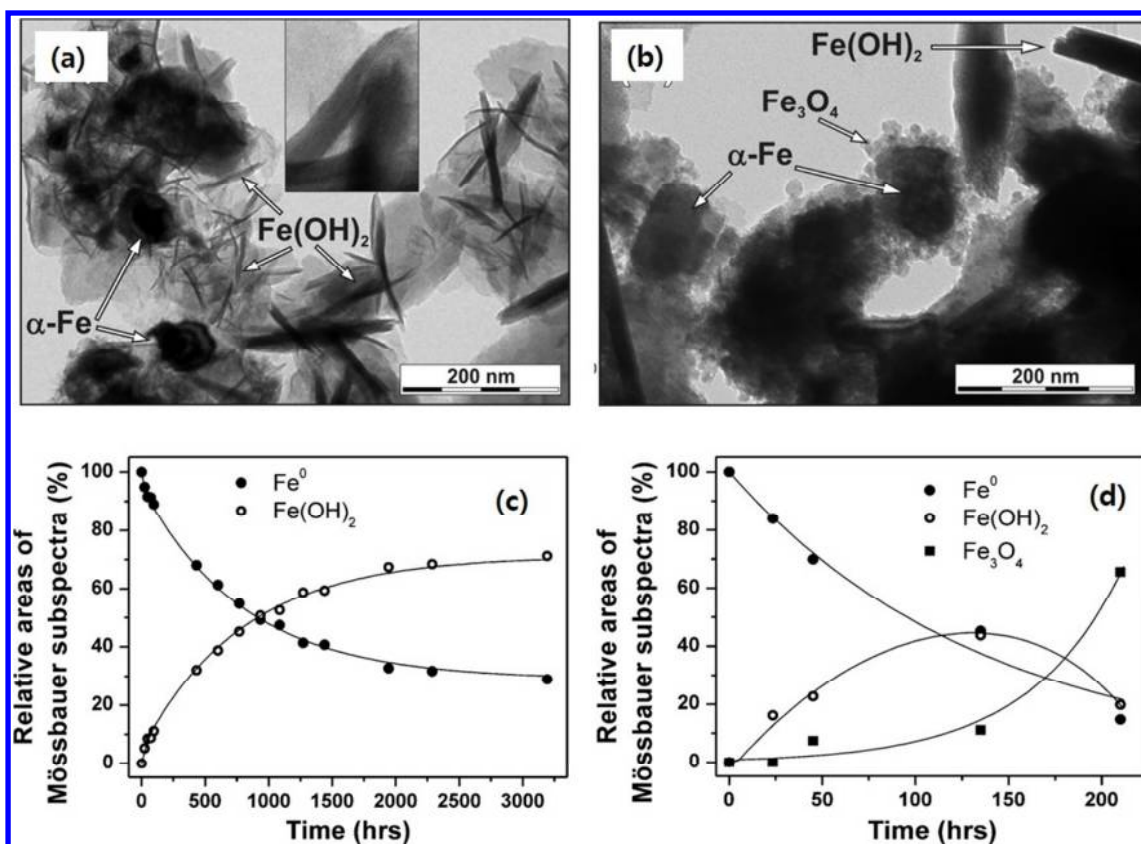


Figure 2.

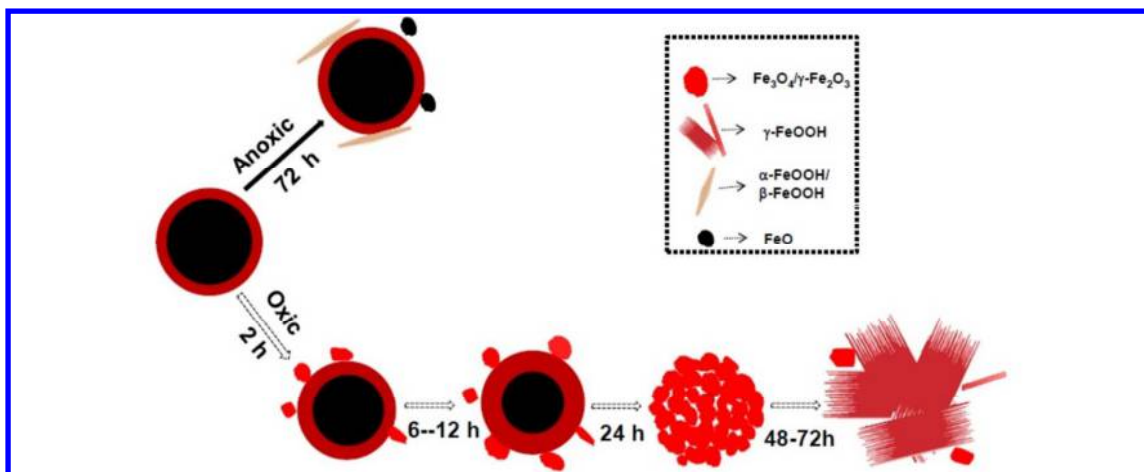


Figure 3.

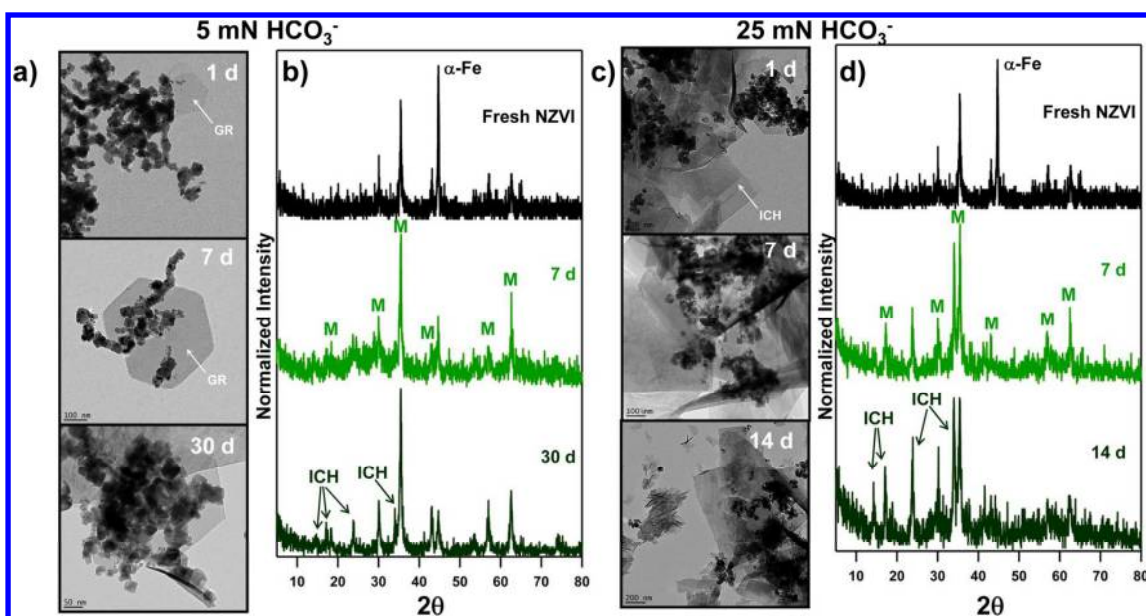


Figure 4.

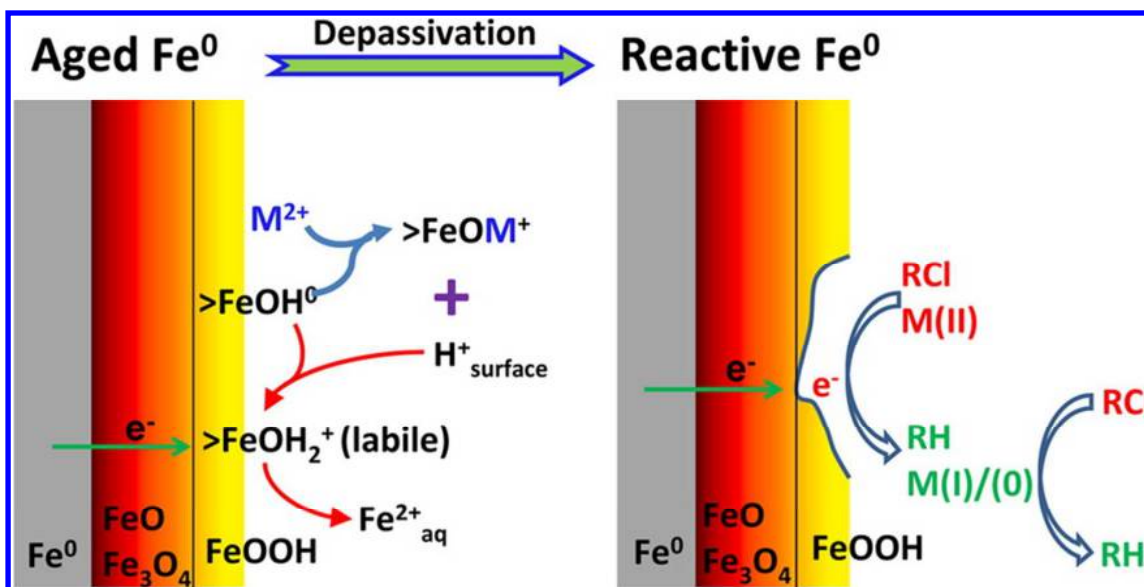


Figure 5.



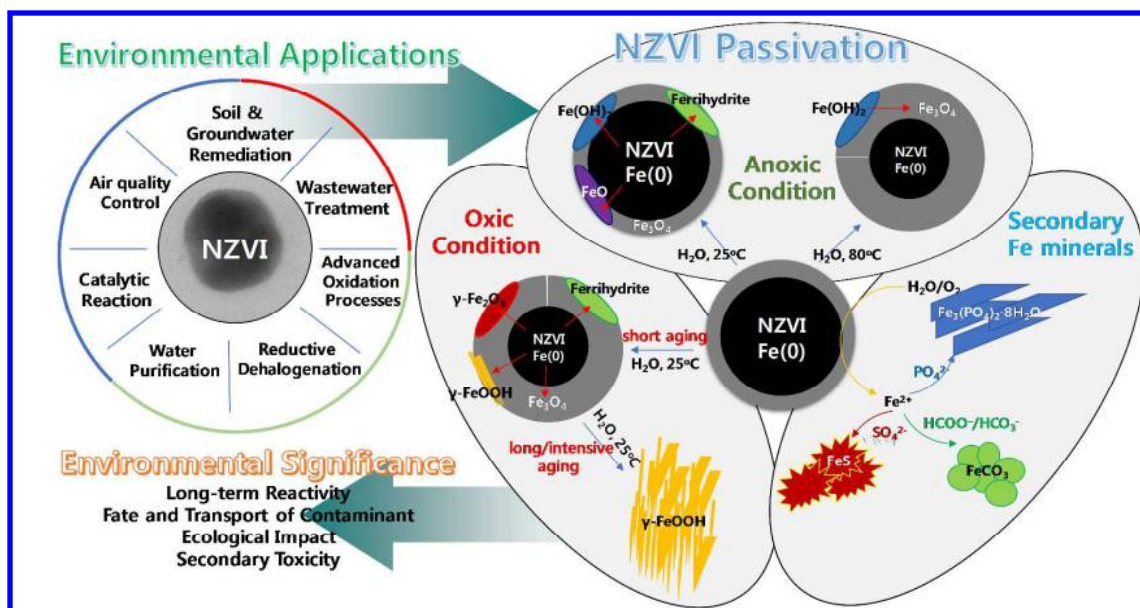


Figure 6.

TOC

